

$X(3872)$ as virtual companion pole of the charm-anticharm state $\chi_{c1}(2P)$

Francesco Giacosa^(a,b), Milena Piotrowska^(a), Susana Coito^(a)

^(a) *Institute of Physics, Jan Kochanowski University,
ul. Świetokrzyska 15, 25-406 Kielce, Poland, and*

^(b) *Institute for Theoretical Physics, Goethe University,
Max-von-Laue-Str. 1, 60438 Frankfurt am Main, Germany.*

We study the spectral function of the axial-vector charmonium state $\chi_{c1}(2P)$ coupled to DD^* mesons, by employing a quantum field theoretical approach: a very pronounced enhancement close to the $D^0 D^{*0}$ threshold, to be identified with the $X(3872)$, emerges. In the complex plane, besides the pole corresponding to a broad seed state, i.e. the $\chi_{c1}(2P)$, in the easiest scenario there is a virtual state (pole on the real axis just below the $D^0 D^{*0}$ threshold on the II Riemann sheet) which corresponds to the $X(3872)$. Our approach describes both the seed state and the dynamically generated $X(3872)$ simultaneously. In particular, it explains the most prominent, both molecular-like and quarkonium-like, features of the $X(3872)$: its very small width is a stable consequence of the approach and the value of the dominant decay into $D^0 D^{*0}$ is predicted to be about 0.5 MeV; the coupling to $\bar{c}c$ is strong, hence prompt production and the enhanced radiative decay into $\psi(2S)\gamma$ w.r.t. $\psi(1S)\gamma$ are natural (predictions for the radiative decays are presented); finally, and most importantly, the isospin breaking decay into $J/\psi\rho$ can be correctly described thanks to DD^* loops mediating this decay channel.

PACS numbers: 11.10.Ef, 12.40.Yx, 14.40.Gx

Keywords: axial-vector charmonia, $X(3872)$, unquenching, effective QCD approaches

I. INTRODUCTION

The axial-vector resonance $X(3872)$, discovered in 2003 by the Belle collaboration [1] and later on confirmed by various experimental collaborations [2], is the first one of a series so-called X, Y, Z states, which do not fit into the simple quark-antiquark picture (see the review papers [3–8] and refs. therein). The state $X(3872)$ is reported in the PDG [2] under the name $\chi_{c1}(3872)$: the average mass is $m_{X(3872)}^{PDG} = 3871.69 \pm 0.17$ MeV, while only an upper limit for the width is given: $\Gamma_{X(3872)}^{PDG} < 1.2$ MeV (90% CL).

The $X(3872)$ is quite unique, since it is very narrow and its mass is very close to the $D^0 D^{*0}$ threshold (it is not yet clear if slightly above or below it). In the $J^{PC} = 1^{++}$ sector, the quark model, using the standard Cornell potential, predicts the existence of a charm-anticharm state $\chi_{c1}(2P)$ at about 3.95 GeV [9–11] (in spectroscopic notation: $n^{2S+1}L_J = 2^3P_1$), which is too high to be straightforwardly identified with the $X(3872)$.

Some features of the $X(3872)$ are very well described by interpreting it as a $D^0 D^{*0}$ molecular state [12–16]: its mass is very close to the $D^0 D^{*0}$ threshold and the isospin-breaking decay $X(3872) \rightarrow J/\psi\rho$ can be understood. (Note, we use $D^0 D^{*0}$ as a shortcut for $D^0 \bar{D}^{*0} + h.c.$). However, some other features, such as the radiative decays and the prompt production of the $X(3872)$ in heavy ion collisions, are better described by a charm-anticharm (or another compact) structure [17–19]. (In what concerns prompt production, there is an ongoing debate, see Refs. [20–24]). In order to account for these different phenomenological aspects, models in which both $\bar{c}c$ and $D^0 D^{*0}$ enter in the wave function of the $X(3872)$ were proposed [25–29]. In other approaches, the $X(3872)$ is described as a compact diquark-antidiquark state, e.g. Ref. [30].

In this work, in line with previous works on the so-called companion poles (see Refs. [31–36] for the light sector and Refs. [37, 38] for the charmonium sector), we follow a different and quite simple idea: instead of working with quark degrees of freedom, a Lagrangian in which a single axial-vector field χ_{c1}^μ , which we identify -in the non-interacting limit- as a $\bar{c}c$ seed state $\chi_{c1} \equiv \chi_{c1}(2P)$ with a bare mass between 3.90 and 3.95 GeV, is considered. This field couples strongly to the $D^0 D^{*0}$ and $D^+ D^{*-}$ meson pairs. As a consequence, the bare seed state is dressed by mesonic quantum fluctuations and acquires a total decay width of about 80 MeV, as predicted by the quark model. We then study the dressed propagator and its imaginary part, which delivers its spectral function. For a suitable but quite natural choice of the coupling of χ_{c1}^μ to DD^* , the spectral function of the charmonium state $\chi_{c1}(2P)$ shows a strong enhancement close to the $D^0 D^{*0}$ threshold. In the easiest scenario, that we put forward here, this enhancement corresponds to a *virtual* state, hence to a pole in the II Riemann sheet (RS) on the real axis and below the lowest $D^0 D^{*0}$ threshold. This pole is interpreted as a companion pole. As expected, the original ‘standard’ seed pole in the III RS (above both thresholds) also exists: its real part is between 3.95 and 4 GeV and its imaginary part is about 35 MeV, in agreement with the predictions of the quark model [9, 17].

The scenario proposed in our work merges quite well both the charmonium and the molecular behavior of the

$X(3872)$. This result is achieved naturally by the mesonic quantum fluctuations dressing the bare state and without considering explicitly the Fock space with both $\bar{q}q$ and molecular components. It is important to stress that there is only one spectral function, correctly normalized to 1, hence strictly speaking there is only ‘one object’. However, the shape of this spectral function is non-trivial and two (relevant) poles on the complex plane are present. Quite interestingly, for certain sets of parameters, the spectral function shows only one peak close to threshold and no peak corresponding to the seed state, thus possibly explaining why the $\bar{c}c$ seed state could not yet be experimentally measured.

Moreover, our study can easily explain why the strong decay into $D^0 D^{*0}$ is dominant (predictions for this decay width are evaluated to be about 0.5 MeV). Moreover, one can understand why radiative decays are in agreement with the charmonium assignment: since $X(3872)$ is part of the spectral function of the whole state $\chi_{c1}(2P)$ (originally a $\bar{c}c$ seed state dressed by DD^* loops), the coupling constants are basically the same (see later for details), hence the decay into $\psi(2S)\gamma$ is larger than the decay into $\psi(1S)\gamma$. For the very same reason, the prompt production of the $X(3872)$ in heavy ion collisions is quite natural. However, due to the close threshold and dressing, various ‘molecular-like’ properties also emerge: the ratio $X(3872) \rightarrow J/\psi\omega \rightarrow J/\psi\pi^+\pi^-\pi^0$ over $X(3872) \rightarrow J/\psi\rho \rightarrow J/\psi\pi^+\pi^-$ can be correctly described by taking into account the small difference between the $D^0 D^{*0}$ and $D^+ D^{*-}$ loop functions.

In the end, it should be stressed that within our approach the very existence of the $X(3872)$ is not possible without the seed charmonium state. If one sends the mass of the latter to infinity and/or reduce the interaction strength to DD^* mesons, the peak associated to $X(3872)$ disappears. This is a feature shared also by works based on quantum mechanics in which the $X(3872)$ was treated as a stationary state defined by a multi-component wave-function with a $\bar{c}c$ coupled to meson-meson channels [26, 28].

The paper is organized as follows: in Sec. II we present the model and in Sec. III the results, divided into strong decays, radiative decays, and isospin-breaking decays. Finally, in Sec. IV we present our conclusions. In addition, in the Appendix A the results for different parameter choices are reported.

II. THE MODEL AND ITS CONSEQUENCES

The Lagrangian: We consider the following Lagrangian that couples a seed state χ_{c1} with quantum numbers 1^{++} (and $n^{2S+1}L_J = 2^3P_1$), to $D^0 \bar{D}^{*0} + h.c.$ and $D^+ D^{*-} + h.c.$ meson pairs:

$$\mathcal{L}_{\chi_{c1}(2P)DD^*} = g_{\chi_{c1}DD^*} \chi_{c1,\mu} [D^{*0,\mu} \bar{D}^0 + D^{*+,\mu} D^- + h.c.] , \quad (1)$$

where:

(i) $g_{\chi_{c1}DD^*}$ is the coupling constant with dimension [Energy] (because of isospin symmetry, it is the same in the neutral and charged channels).

(ii) The theory is regularized via a form factor $F_\Lambda(k)$, which takes effectively into account the finite dimensions of the mesons and their interactions (microscopically, there is a nonlocal triangle diagram involving two c quarks and one light quark [39]). The tree-level decay widths as function of the ‘running mass’ m of χ_{c1} read:

$$\Gamma_{\chi_{c1}(2P) \rightarrow D^{*0} \bar{D}^0 + h.c.}(m) = 2 \frac{k(m, m_{D^{*0}}, m_{D^0})}{8\pi m^2} \frac{g_{\chi_{c1}DD^*}^2}{3} \left(3 + \frac{k^2(m, m_{D^{*0}}, m_{D^0})}{m_{D^{*0}}^2} \right) F_\Lambda(k) , \quad (2)$$

$$\Gamma_{\chi_{c1}(2P) \rightarrow D^{*+} D^- + h.c.}(m) = 2 \frac{k(m, m_{D^{*+}}, m_{D^+})}{8\pi m^2} \frac{g_{\chi_{c1}DD^*}^2}{3} \left(3 + \frac{k^2(m, m_{D^{*+}}, m_{D^+})}{m_{D^{*+}}^2} \right) F_\Lambda(k) , \quad (3)$$

where $k \equiv k(m, m_1, m_2)$ is the modulus of the three-momentum of an emitted particle (m is the mass of the decaying particle and m_1 and m_2 the masses of the decay products).

(iii) We choose a Gaussian form factor,

$$F_\Lambda(k) = e^{-\frac{2k^2(m, m_1, m_2)}{\Lambda^2}} , \quad (4)$$

since it emerges quite naturally in the 3P_0 model from the overlap of the mesonic wave functions (e.g. Refs. [40–45]). The precise form of $F_\Lambda(k)$ has a small influence on the results, as long as it is a smooth function which guarantees convergence, see the detailed discussion in Refs. [36–38, 46]. As shown in Ref. [47], covariance is fulfilled even when using a form factor that cuts the three-momentum k (such as in Eq. (4)), provided that this form is used only in the reference frame in which the decaying particle is at rest. In the Appendix A we will also use, for comparison and for completeness, a different vertex.

(iv) The numerical value of Λ is quite important. Typically, it ranges from 0.4 to 0.8 GeV [35, 36, 39, 45]. Note, Λ should not be regarded as a cutoff of a fundamental theory, but as a parameter which is inversely proportional to the radius of mesons. We shall start with 500 MeV (typical for mesonic objects [36, 38]), but as we find qualitatively similar results by varying Λ in the above mentioned range (see the Appendix A).

(v) The theory, together with the form factor, is finite. For each value of m (and hence of the momentum k) the model is mathematically well defined (no matter how large m is). In fact, the normalization of the spectral function in Eq. (11) (see below) is realized by formally integrating up to infinity. Of course, far from the energy of interest, the model - even if mathematically well defined - cannot represent a reliable description of reality, since other resonances are missing. We thus consider our approach valid up to $m \lesssim 4$ GeV. The important point, however, is that we do not require that k should be smaller than Λ : simply, when k is larger than Λ , that decay mode is naturally suppressed. Similarly, in the already mentioned 3P_0 model, it is common to have values of k larger than Λ [43].

The propagator and the spectral function: The scalar part of the propagator of the field χ_{c1} , as function of the variable $s = m^2$, reads:

$$\Delta(s) = \frac{1}{s - m_0^2 + \Pi(s)} , \quad (5)$$

where $m_0 \approx 3.95$ GeV is the bare quark-antiquark mass of χ_{c1} predicted by quark models [9]. The quantity

$$\Pi(s) = \Pi_{D^{*0}\bar{D}^0+h.c.}(s) + \Pi_{D^{*+}D^-+h.c.}(s) = g_{\chi_{c1}DD^*}^2 [\Sigma_{D^{*0}\bar{D}^0+h.c.}(s) + \Sigma_{D^{*+}D^-+h.c.}(s)] \quad (6)$$

is the self-energy contribution, which is the sum of the $D^{*0}\bar{D}^0$ and $D^{*+}D^-$ loops. We note that, at the one-loop level, the quantities $\Sigma_{D^{*0}\bar{D}^0+h.c.}$ and $\Sigma_{D^{*+}D^-+h.c.}$, defined in Eq. (6), do not depend on the coupling constant $g_{\chi_{c1}DD^*}^2$. As shown in Ref. [48], the one-loop level is a very good approximation for hadronic phenomenology (no need to consider diagrams in which the unstable state is exchanged by the decay products).

At one-loop, the imaginary part reads

$$\text{Im } \Pi(s) = \sqrt{s} [\Gamma_{\chi_{c1}(2P) \rightarrow D^{*0}\bar{D}^0+h.c.}(\sqrt{s}) + \Gamma_{\chi_{c1}(2P) \rightarrow D^{*+}D^-+h.c.}(\sqrt{s})] . \quad (7)$$

The real part is obtained by the following dispersion relation (valid for \sqrt{s} real and larger than $m_{D^{*+}} + m_{D^-}$) :

$$\begin{aligned} \text{Re } \Pi(s) &= \frac{PP}{\pi} \int_{(m_{D^{*0}}+m_{D^0})^2}^{\infty} \frac{\sqrt{s'} \Gamma_{\chi_{c1}(2P) \rightarrow D^{*0}\bar{D}^0+h.c.}(\sqrt{s'})}{s' - s} ds' \\ &+ \frac{PP}{\pi} \int_{(m_{D^{*+}}+m_{D^+})^2}^{\infty} \frac{\sqrt{s'} \Gamma_{\chi_{c1}(2P) \rightarrow D^{*+}D^-+h.c.}(\sqrt{s'})}{s' - s} ds' . \end{aligned} \quad (8)$$

For $s < (m_{D^{*0}} + m_{D^0})^2$ or having a nonzero imaginary part, PP is omitted and $\Pi(s = z^2)$, in the I Riemann sheet (RS), is:

$$\Pi(s = z^2) = \frac{1}{\pi} \int_{(m_{D^{*0}}+m_{D^0})^2}^{\infty} \frac{\sqrt{s'} \Gamma_{\chi_{c1} \rightarrow D^{*0}\bar{D}^0+h.c.}(\sqrt{s'})}{s' - z^2} ds' + \frac{1}{\pi} \int_{(m_{D^{*+}}+m_{D^+})^2}^{\infty} \frac{\sqrt{s'} \Gamma_{\chi_{c1} \rightarrow D^{*+}D^-+h.c.}(\sqrt{s'})}{s' - z^2} ds' . \quad (9)$$

It should be stressed that $\Pi(z^2 \rightarrow \infty) \rightarrow 0$ in all directions of the complex plane. In order to avoid misunderstanding, we recall that, in the I RS, the function $\Pi(z^2 \rightarrow \infty)$ is an utterly different complex function than e^{-z^2/Λ^2} , see Ref. [37] for a detailed discussion of this point. In fact, in the I RS, besides the cut along the real axis, $\Pi(z^2)$ is regular and well defined everywhere and does not contain any singular point, contrary to e^{-z^2/Λ^2} , which contains an essential singularity at ∞ . In other Riemann sheets, the properties of $\Pi(z^2)$ are different and singular points are present.

The spectral function (or the mass distribution) is defined as

$$d_{\chi_{c1}(2P)}(m) = -\frac{2m}{\pi} \text{Im}[\Delta(s = m^2)] . \quad (10)$$

The quantity $\text{dmd}_{\chi_{c1}(2P)}(m)$ represents the probability that the unstable state has a mass between m and $m + \text{dm}$

[46, 49–51]. It fulfills the important normalization condition

$$\int_{m_{D^{*0}} + m_{D^0}}^{\infty} dm \, d_{\chi_{c1}(2P)}(m) = 1 . \quad (11)$$

This is a consequence of the Källén–Lehmann representation and of unitarity. For a rigorous proof, using the vertex function regularization (and for the link to other regularization schemes), see Ref. [50]. In our approach, the normalization follows automatically from the formalism. The numerical verification of Eq. (11) represents an important check of the correctness of the numerically performed calculations.

The definition(s) of the mass(es): An unstable state is described by its mass distribution and, strictly speaking, it does not have a definite mass. Nevertheless, one can define it in various ways. A typical one is the so-called Breit-Wigner (BW) mass, given by $\text{Re}[\Delta^{-1}(s = m_{BW}^2)] = 0$. This equation is however meaningful when a unique and symmetric peak of the spectral function is present. As we shall see, this is not true in our case. Alternatively, it is common to search for the position(s) of the pole(s) in the complex plane $\Delta^{-1}(s = z_{pole}^2) = 0$ and then identify the mass as its real part, $m_{pole} = \text{Re}[z_{pole}]$ (in the proper Riemann sheet). Here, this second approach is more useful for both poles, the standard $\bar{c}c$ one, in the III RS, and the virtual one, linked to $X(3872)$, on the II RS.

Radiative decays: Besides the dominant decay into DD^* , the terms that describe the radiative decays read:

$$\mathcal{L}_{\chi_{c1}\text{-rad}} = g_{\chi_{c1}\psi(1S)\gamma} \chi_{c1,\mu}\psi(1S)_{\nu}\tilde{F}^{\mu\nu} + g_{\chi_{c1}\psi(2S)\gamma} \chi_{c1,\mu}\psi(2S)_{\nu}\tilde{F}^{\mu\nu} + \dots , \quad (12)$$

where the coupling constants $g_{\chi_{c1}\psi(1S)\gamma}$ and $g_{\chi_{c1}\psi(2S)\gamma}$ can be determined by the quark model [17] (through the overlap of wave functions). Later on, we shall use the couplings determined in Ref. [17].

III. RESULTS

In this Section, we present the results by starting from the spectral functions, poles, and strong decays (Sec. III A). Later on, we focus on radiative decays, prompt production, and isospin breaking decays (Sec. III B).

A. Spectral function, poles, and strong decays

Case I ($m_0 = 3.95$ GeV): As a first case, let us set the bare mass to $m_0 = 3.95$ GeV (close to the value predicted by the quark model in Ref. [9]). For the parameter Λ we shall use 0.5 GeV (this is a typical value for Λ ; later, we will check the dependence on Λ). The masses of the pseudoscalar states read $m_{D^0} = 1.86483$ GeV and $m_{D^+} = 1.86959$ GeV, and the masses of the vector states are $m_{D^{*0}} = 2.00685$ GeV and $m_{D^{*+}} = 2.01026$ GeV. Hence, the relevant thresholds are: $m_{D^0} + m_{D^{*0}} = 3.87168$ GeV and $m_{D^+} + m_{D^{*+}} = 3.87985$ GeV.

We determine the coupling constant $g_{\chi_{c1}DD^*} = 9.732$ GeV by requiring that:

$$\text{Re}[\Delta^{-1}(s = m_*^2)] = 0, \text{ for } m_* = 3.874 \text{ GeV} . \quad (13)$$

The chosen value of m_* is slightly *above* the $D^{*0}D^0$ threshold, but below the $D^{*+}D^-$ one. Again, the precise value of m_* is not so important, as long as it is between the two thresholds (see below).

The spectral function $d_{\chi_{c1}(2P)}(m)$ is plotted in Fig. 1. It has a very peculiar form: a extremely narrow and high peak *very* close to the $D^{*0}D^0$ threshold is realized. We identify this peak with the resonance $X(3872)$. A second and broad peak at 3.986 GeV is also visible, and it corresponds to a roughly 80 MeV broad state, in agreement with old and recent quark model predictions. It should be however stressed that the whole spectral function of Fig. 1, even if it contains two peaks, originates from one single seed state, and it is correctly normalized to 1, as we verify numerically upon integrating to 10 GeV (much larger than the energy scale involved, hence *de facto* infinity). This in turn shows that, as anticipated, the model is mathematically consistent up to large values.

Between the thresholds one has:

$$\int_{m_{D^{*0}} + m_{D^0}}^{m_{D^+} + m_{D^{*+}}} dm \, d_{\chi_{c1}(2P)}(m) = 0.160 , \quad (14)$$

thus 16% of the whole spectral function is contained in this energy interval. Yet, since the $X(3872)$ is definitely narrower than 8 MeV, and the experimental uncertainty of its width is roughly 1 MeV, we also consider the integral

$$\int_{m_{D^*0}+m_{D^0}}^{m_{D^*0}+m_{D^0}+1 \text{ MeV}} dm d_{\chi_{c1}(2P)}(m) = 0.049 , \quad (15)$$

that we interpret as it follows: the $X(3872)$ corresponds roughly to 4.9% of the whole object described by $d_{\chi_{c1}(2P)}(m)$. In other parts of the work, we shall repeat the ‘1 MeV’ estimate for the extension of the peak associated to the $X(3872)$.

In Fig. 2, we plot the function $\text{Re}[\Delta^{-1}(s = m^2)]$: by construction, it has a zero at $m_* = 3.874$ GeV, which is responsible for the high peak associated with the $X(3872)$, at the $D_0 D_0^*$ threshold. There is another zero at $m = 3.973$ GeV, corresponding to the broad peak on the right. A third zero, at 3.891 GeV, does not correspond to any peak, since the derivative of the function is negative (see the discussion in Ref. [31]).

As expected, there is a pole on the III RS, which comes from the $\bar{c}c$ seed state, that relates to the broad peak:

$$3.995 - i0.036 \text{ GeV} . \quad (16)$$

Thus, a pole width of 72 MeV follows. In addition, a virtual state is obtained: there is a pole on the II RS on the real axis, just below the $D^{*0} D^0$ threshold, for:

$$3.87164 - i\varepsilon \text{ GeV} . \quad (17)$$

This is the pole associated to $X(3872)$, appearing as a narrow peak above the threshold in Fig. 1.

Summarizing:

$$X(3872) \Leftrightarrow \begin{cases} \text{zero of } \text{Re}[\Delta^{-1}(s = m^2)] \text{ for } m_* = 3.874 \text{ GeV} \\ \text{virtual pole on the II RS for } 3.87164 - i\varepsilon \text{ GeV} \end{cases} . \quad (18)$$

Note, the virtual pole is just 0.04 MeV below the $D^0 D^{*0}$ threshold. Of course, the precise value of m_* and the virtual pole vary when changing the parameters, but the overall picture is quite stable.

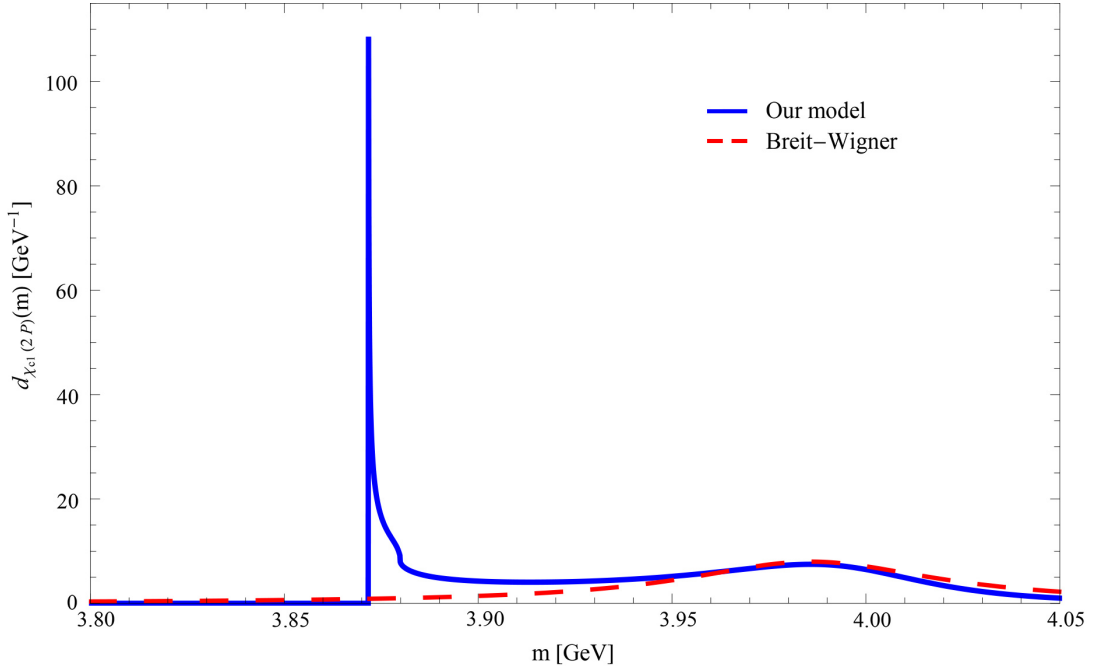


FIG. 1: Solid line: spectral function $d_{\chi_{c1}(2P)}(m)$ in Eq. (10), for the case I (see text). Two peaks are present, linked to two distinct poles. A broad peak, originated by the seed $\bar{c}c$ state, at about 3.99 GeV is present on the right, while a narrow and high peak is located just on the right of the lowest threshold: it results from DD^* loops dressing the $\bar{c}c$, and corresponds to the well known state $X(3872)$. The dashed line corresponds to a Breit-Wigner approximation for the seed state, with parameters $m_{BW} = 3.986$ GeV and $\Gamma_{BW} = 79.7$ MeV (cf. Eqs. (19) and (20)).

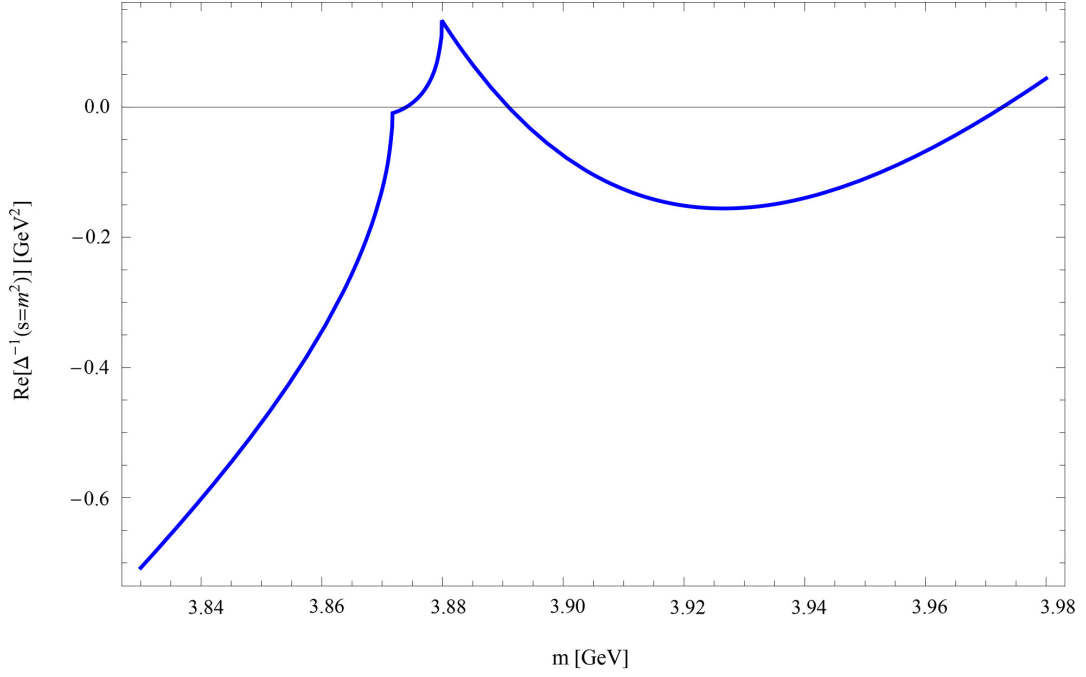


FIG. 2: Plot of the function $\text{Re}[\Delta^{-1}(m^2)]$ (see Eq. (5)) for case I (see text). Three zeros are present: on the right for $m = 3.973$ GeV, which corresponds roughly to the broad peak of the spectral function, and to the pole in the III RS of the ‘seed’ charmonium 2^3P_1 state; on the left for $m_* = 3.874$ GeV (in between the thresholds), which corresponds to the narrow peak at the $D^0\bar{D}^{*0}$ threshold and to a virtual pole on the II RS; the zero in the middle does not lead to peaks or poles.

Next, we turn to decay widths. From Fig. 1, it is clear that the spectral function has not a Breit-Wigner form. Nevertheless, for the maximal height of the broad peak, which is located at 3.986 GeV, reasonable estimates are found:

$$\Gamma_{\chi_{c1}(2P) \rightarrow D^{*0}\bar{D}^0 + h.c.}(3.986 \text{ GeV}) = 38.1 \text{ MeV} , \quad (19)$$

$$\Gamma_{\chi_{c1}(2P) \rightarrow D^{*+}D^- + h.c.}(3.986 \text{ GeV}) = 41.6 \text{ MeV} , \quad (20)$$

for a total width of 79.7 MeV: this is the width used for the Breit-Wigner function in Fig. 1 (note, using the pole mass would generate similar results).

For the peak close to threshold, identified with $X(3872)$, a direct evaluation of the width at the peak is not really useful. The peak itself has a very small width at half height (~ 0.1 MeV). Even when changing the parameters, it is always smaller than 0.5 MeV. As a good estimate of the dominant decay of the $X(3872)$, we consider the following average value, which extends from the threshold to the left-threshold plus 1 MeV, that includes the peak:

$$\Gamma_{X(3872) \rightarrow D^{*0}\bar{D}^0 + h.c.}^{\text{average}} = \int_{m_{D^{*0}} + m_{D^0}}^{m_{D^{*0}} + m_{D^0} + 1 \text{ MeV}} dm \Gamma_{\chi_{c1}(2P) \rightarrow D^{*0}\bar{D}^0 + h.c.}(m) d_{\chi_{c1}(2P)}(m) = 0.61 \text{ MeV}. \quad (21)$$

Thus, the model shows that the decay of $X(3872)$ into $D^{*0}\bar{D}^0 + h.c.$ is sizable: in fact, 0.61 MeV is comparable to the maximal value of about 1 MeV, estimated for the $X(3872)$. On the other hand, $\Gamma_{X(3872) \rightarrow D^{*+}D^- + h.c.}$ vanishes because $X(3872)$ is always subthreshold for this decay channel.

In the Appendix A, we discuss the results for other parameter choices, for which there are no big qualitative changes: the overall picture is quite stable. The variation of the results also represents an estimate of the uncertainties of our analysis. In A 2, we repeat the study for different values of Λ , and keep $m_* = 3.874$ GeV fixed by adjusting the coupling constant. On the other hand, in A 1 we change the coupling constant $g_{\chi_{c1}DD^*}$, and keep Λ fixed by varying m_* . For smaller couplings, m_* moves to the right threshold $m_{D^+} + m_{D^{*+}}$, and the height of the peak $X(3872)$ decreases and gradually fades away. When $g_{\chi_{c1}DD^*}$ becomes too small, m_* exceeds $m_{D^+} + m_{D^{*+}}$ and the peak associated to the $X(3872)$ disappears. When $g_{\chi_{c1}DD^*}$ increases, m_* moves to the left towards the $D^{*0}D^0$ threshold, and the height of the $X(3872)$ increases. For coupling constants exceeding the critical value $g_{\chi_{c1}DD^*}^{\text{critical}} = 9.808$ GeV, for which m_* lies just at the $m_{D^{*0}} + m_{D^0}$ threshold, there is a pole in the first Riemann sheet: an additional (quasi-)stable bound state

emerges. In such case, the spectral function takes the form [46]:

$$d_{\chi_{c1}(2P)}(m) = Z\delta(m - m_{BS}) + d_{\chi_{c1}(2P)}^{\text{above threshold}}(m) \quad (22)$$

where m_{BS} is the mass of the bound-state, to be interpreted as a dynamically generated molecular-like state (still, this bound state is deeply connected to the seed state and cannot exist without it). The normalization (11) is still formally valid, leading to:

$$Z + \int_{m_{D^*0} + m_{D^0}}^{\infty} dm d_{\chi_{c1}(2P)}^{\text{above threshold}}(m) = 1. \quad (23)$$

For instance, for $g_{\chi_{c1}DD^*} = 10$ GeV (just above the critical value), one has $Z = 0.0465$ and $m_{BS} = 3.87164$ GeV (hence, this is a pole on the I RS). The shape of $d_{\chi_{c1}(2P)}^{\text{above threshold}}$ is very similar to Fig. 1, with the important difference that the area does not sum up to unity. It is then very difficult to distinguish the case in Fig. 1 from this latter one, even if there is an important difference: *virtual* versus *real* pole. A (quasi-)bound state, below threshold, neither decays into $D^{*0}D^0$ nor into $D^{*+}D^-$, but only into suppressed radiative and light hadron decays, thus the width associated to this pole is very small, but the peak just above the D^0D^{*0} threshold is still present. Note, the integral of the function $d_{\chi_{c1}(2P)}^{\text{above threshold}}(m)$, between the two thresholds, amounts to 0.133, while between $m_{D^*0} + m_{D^0}$ and $m_{D^*0} + m_{D^0} + 1$ MeV to 0.035, thus slightly smaller than the previous case reported in Eq. (15).

Case II ($m_0 = 3.92$ GeV): We repeat the study for a different value of the bare mass m_0 . We use $m_0 = 3.92$ GeV, slightly smaller than the value in Ref. [9] and close to the value in Ref. [11]. We determine the coupling constant $g_{\chi_{c1}DD^*} = 7.557$ GeV by requiring, as before, that $m_* = 3.874$ GeV. The spectral function is depicted in Fig. 3. There is still a very pronounced peak close to the D^0D^{*0} threshold, but there is no peak at higher values: the broad peak corresponding to the seed melts with the whole structure (for a similar result, see [29, 52]).

The amount of spectral function between the thresholds is:

$$\int_{m_{D^*0} + m_{D^0}}^{m_{D^*+} + m_{D^{*+}}} dm d_{\chi_{c1}(2P)}(m) = 0.250, \quad (24)$$

while the one associated to the $X(3872)$ is

$$\int_{m_{D^*0} + m_{D^0}}^{m_{D^*0} + m_{D^0} + 1 \text{ MeV}} dm d_{\chi_{c1}(2P)}(m) = 0.067. \quad (25)$$

In Fig. 4 we also plot $\text{Re}[\Delta^{-1}(s = m^2)]$. As required, there is one zero at 3.874 GeV. However, no other intersection is present: this is in agreement with the absence of the broad peak in Fig. 3. Even if there is no peak, there is indeed a pole on the III Riemann sheet (seed state):

$$3.953 - i0.044 \text{ GeV}, \quad (26)$$

pretty similar to the case I presented in Eq. (16). Thus, a pole width of 88 MeV follows. This example shows how important it is to look for poles: a state may exist even when there is no bump. In addition, a virtual state on the II RS is obtained for:

$$3.87160 - i\epsilon \text{ GeV}, \quad (27)$$

just 0.08 MeV below the \bar{D}^0D^{*0} threshold.

Let us turn to the partial widths. Since there is no peak, we use the pole value of 3.953 GeV for the on-shell mass:

$$\Gamma_{\chi_{c1}(2P) \rightarrow D^{*0}\bar{D}^0 + h.c.}(3.953) = 32.9 \text{ MeV}, \quad (28)$$

$$\Gamma_{\chi_{c1}(2P) \rightarrow D^{*+}D^- + h.c.}(3.953) = 35.4 \text{ MeV}. \quad (29)$$

The peak close to threshold, denoted as $X(3872)$, has a width at half height of ~ 0.91 MeV. The integrated signal

$$\Gamma_{X(3872) \rightarrow D^{*0}\bar{D}^0 + h.c.}^{\text{average}} = \int_{m_{D^*0} + m_{D^0}}^{m_{D^*0} + m_{D^0} + 1 \text{ MeV}} dm \Gamma_{\chi_{c1}(2P) \rightarrow D^{*0}\bar{D}^0 + h.c.}(m) d_{\chi_{c1}(2P)}(m) = 0.54 \text{ MeV} \quad (30)$$

is very similar to case I. This is in general a quite stable outcome of our study.

Increasing and decreasing the cutoff Λ and the coupling constant $g_{\chi_{c1}DD^*}$ generates the same type of changes mentioned above, see the Appendix A for further details.

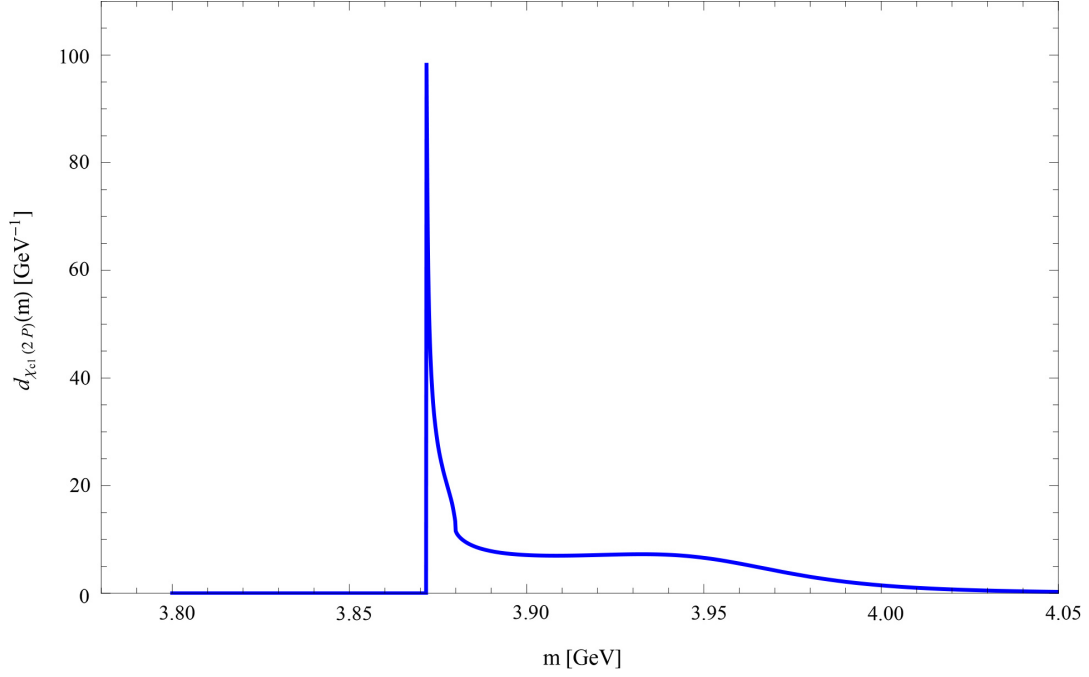


FIG. 3: Solid line: spectral function for case II (see text). As it is visible, there is no peak for the seed state, but the pronounced peak corresponding to $X(3872)$ still exists.

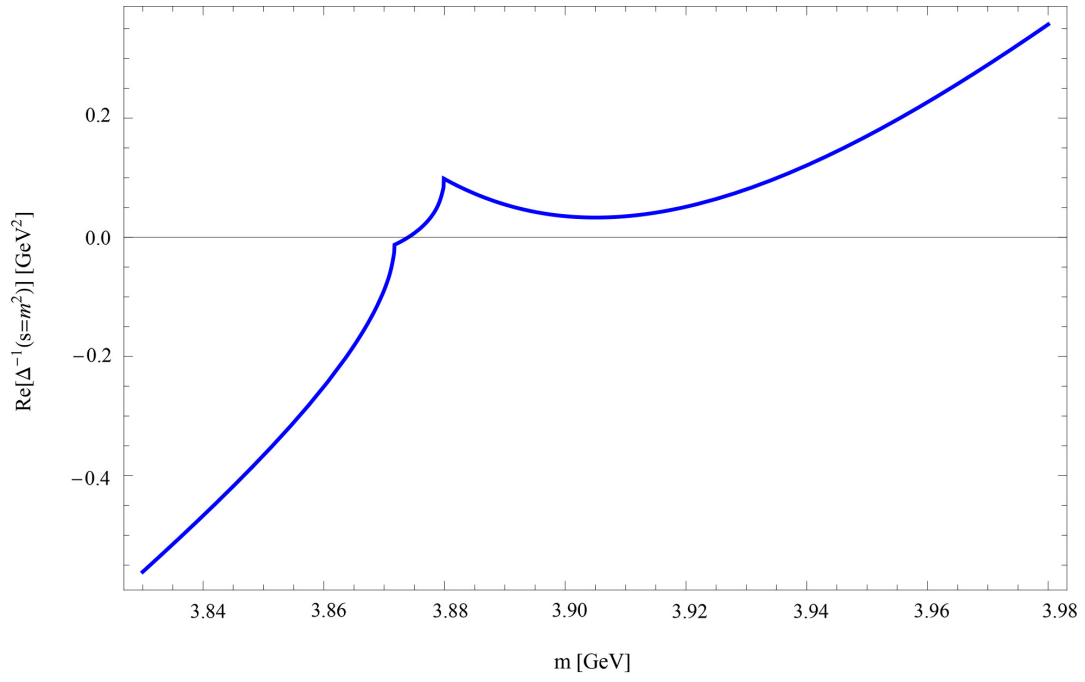


FIG. 4: Plot of the function $\text{Re}[\Delta^{-1}(m^2)]$ (see Eq. (5)) for case II (see text). Only one zero at $m_* = 3.874$ GeV (in between the thresholds) is present, which corresponds to the narrow peak at the $D^0 D^{*0}$ threshold and to a virtual pole on the II RS.

B. Consequences of the approach

Next, we study various consequences of the approach: radiative decays, prompt production, and, most notably, the isospin-breaking strong decay. We use the numerical values of case I in Sec. III A. For other parameter choices, see the Appendix A.

Radiative decays: The coupling constants $g_{\chi_{c1}(2P)\psi(1S)\gamma}$ and $g_{\chi_{c1}(2P)\psi(2S)\gamma}$, entering Eq. (12) and describing the radiative transitions $\chi_{c1}(2P) \rightarrow \psi(1S)\gamma$ and $\chi_{c1}(2P) \rightarrow \psi(2S)\gamma$, can be calculated within the quark model. They are proportional to the overlap of the spatial wave functions of $\chi_{c1}(2P)$ with, respectively, $\psi(1S)$ and $\psi(2S)$. It follows that $g_{\chi_{c1}(2P)\psi(2S)\gamma}$ is larger than $g_{\chi_{c1}(2P)\psi(1S)\gamma}$, since the $2P \rightarrow 2S$ overlap is larger than $2P \rightarrow 1S$ (this is due to the fact that in the latter a cancellation due to the node, present only in $2P$, occurs).

The decay widths of the processes $\chi_{c1}(2P) \rightarrow \psi(1S)\gamma$ and $\chi_{c1}(2P) \rightarrow \psi(2S)\gamma$, as a function of the running mass m of $\chi_{c1}(2P)$, read:

$$\Gamma_{\chi_{c1}(2P) \rightarrow \psi(1S)\gamma}(m) = g_{\chi_{c1}(2P)\psi(1S)\gamma}^2 \frac{k^3(m, m_{\psi(1S)}, 0)}{8\pi m^2} \frac{4}{3} \left(1 + \frac{k^2(m, m_{\psi(1S)}, 0)}{m_{\psi(1S)}^2} \right), \quad (31)$$

$$\Gamma_{\chi_{c1}(2P) \rightarrow \psi(2S)\gamma}(m) = g_{\chi_{c1}(2P)\psi(2S)\gamma}^2 \frac{k^3(m, m_{\psi(2S)}, 0)}{8\pi m^2} \frac{4}{3} \left(1 + \frac{k^2(m, m_{\psi(2S)}, 0)}{m_{\psi(2S)}^2} \right). \quad (32)$$

Hence, their ratio is

$$\frac{\Gamma_{\chi_{c1}(2P) \rightarrow \psi(2S)\gamma}(m)}{\Gamma_{\chi_{c1}(2P) \rightarrow \psi(1S)\gamma}(m)} = \left(\frac{g_{\chi_{c1}(2P)\psi(2S)\gamma}}{g_{\chi_{c1}(2P)\psi(1S)\gamma}} \right)^2 \left(\frac{k(m, m_{\psi(2S)}, 0)}{k(m, m_{\psi(1S)}, 0)} \right)^3 \left(\frac{1 + \frac{k^2(m, m_{\psi(2S)}, 0)}{m_{\psi(2S)}^2}}{1 + \frac{k^2(m, m_{\psi(1S)}, 0)}{m_{\psi(1S)}^2}} \right). \quad (33)$$

Following Ref. [17], $g_{\chi_{c1}(2P)\psi(2S)\gamma} \propto \sqrt{\alpha_{QED}} \langle 2S | r | 2P \rangle$ and $g_{\chi_{c1}(2P)\psi(1S)\gamma} \propto \sqrt{\alpha_{QED}} \langle 1S | r | 2P \rangle$, where the numerical values are $\langle 2S | r | 2P \rangle \simeq 2.72 \text{ GeV}^{-1}$ and $\langle 1S | r | 2P \rangle \simeq 0.15 \text{ GeV}^{-1}$ [17]. We recall that $\chi_{c1}(2P)$ in Eq. (33) refers to the whole energy domain of the state. For the decays of $X(3872)$, we set $m \simeq m_{X(3872)} \simeq 3.872 \text{ GeV}$: we obtain $\frac{\Gamma_{X(3872) \rightarrow \psi(2S)\gamma}}{\Gamma_{X(3872) \rightarrow \psi(1S)\gamma}} \simeq 5.4$. This is comparable to (but somewhat larger than) the experimental value 2.6 ± 0.4 reported by the PDG [2]. We also recall the values $2.38 \pm 0.64 \pm 0.29$, determined by the LHCb collaboration [53] and 3.4 ± 1.4 , determined by the BABAR collaboration [54] (see also the theoretical discussion in Ref. [55]).

The main point concerning the radiative decays is that our approach naturally explains the large $\psi(2S)\gamma$ to $\psi(1S)\gamma$ ratio, since the $\bar{c}c$ component provides the dominant contribution to these decays, see Eq. (12). Thus, this feature applies for both the seed state and for $X(3872)$. On the contrary, a purely molecular state would deliver the opposite result: $\langle 2S | r | 2P \rangle$ much smaller than $\langle 1S | r | 2P \rangle$. Yet, as discussed in Ref. [56], a DD^* component is not excluded. (Indeed, our slight overestimation of the ratio can be caused by not considering DD^* loop processes in a way similar to the isospin breaking decays described below).

Finally, we use our approach to estimate the decay widths for the two channels, upon integrating over the spectral function:

$$\Gamma_{X(3872) \rightarrow \psi(1S)\gamma} = \int_{m_{D^*0} + m_{D^0}}^{m_{D^*0} + m_{D^0} + 1 \text{ MeV}} dm \Gamma_{\chi_{c1}(2P) \rightarrow \psi(1S)\gamma}(m) d_{\chi_{c1}(2P)}(m) \simeq 0.54 \text{ keV}, \quad (34)$$

$$\Gamma_{X(3872) \rightarrow \psi(2S)\gamma} = \int_{m_{D^*0} + m_{D^0}}^{m_{D^*0} + m_{D^0} + 1 \text{ MeV}} dm \Gamma_{\chi_{c1}(2P) \rightarrow \psi(2S)\gamma}(m) d_{\chi_{c1}(2P)}(m) \simeq 3.13 \text{ keV}, \quad (35)$$

where we have used the coupling constants $g_{\chi_{c1}(2P)\psi(2S)\gamma} = 1.737$ and $g_{\chi_{c1}(2P)\psi(1S)\gamma} = 0.093$, extracted from Ref. [17]. These widths are predictions of our approach for the radiative decays.

Prompt production: Within our interpretation of the $X(3872)$, its production in heavy ion collisions can be easily explained. The reason is that the $\bar{c}c$ system, dressed by DD^* clouds, can be regarded as a single object described by the whole spectral function in Fig. 1, even if it leads to two poles, and thus two states. As seen for radiative decays, whatever the bare coupling to the state $\chi_1(2P)$ is, the very same coupling holds in general for the broad peak coming from the seed and also for the narrow peak corresponding to the $X(3872)$.

Note, a different question is the role of this resonance in thermal models. In agreement with the case studied of Ref. [57], the resonance $X(3872)$ is expected to be subleading [58]. (For the appropriate theoretical framework, see e.g. Refs. [59–61] and refs. therein.)

Isospin breaking decay: The decay $\chi_1(2P) \rightarrow \psi(1S)\omega \rightarrow \psi(1S)\pi^+\pi^-\pi^0$ can take place via two different mechanisms: the first involves the emission of two gluons, which then convert into an ω , while the second involves the DD^* loops which couple to $\psi(1S)\omega$.

On the contrary, at a first sight, the decay $\chi_1(2P) \rightarrow \psi(1S)\rho^0 \rightarrow \psi(1S)\pi^+\pi^-$ cannot occur, since it violates isospin. The two-gluon mechanism is not possible, since two gluons cannot convert into a ρ meson. Yet, the DD^* loop generates an isospin-suppressed coupling of $\chi_1(2P)$ to $\psi(1S)\rho$, as we shall discuss below.

In order to show these aspects, let us consider the following Lagrangian coupling DD^* to ω and ρ^0 :

$$\mathcal{L}_{DD^*} = \xi_0 D^{*0\mu} \bar{D}^0 \psi(1S)^\nu [\tilde{\omega}_{\mu\nu} + \tilde{\rho}_{\mu\nu}^0] + \xi_0 D^{*+\mu} D^- \psi(1S)^\nu [\tilde{\omega}_{\mu\nu} - \tilde{\rho}_{\mu\nu}^0] + h.c. , \quad (36)$$

where $\tilde{\omega}_{\mu\nu} + \tilde{\rho}_{\mu\nu}^0$ is proportional to $\bar{u}u$ (and hence couples to $D^0\bar{D}^0$), while $\tilde{\omega}_{\mu\nu} - \tilde{\rho}_{\mu\nu}^0$ to $\bar{d}d$ (and hence couples to $D^{*+}D^-$). The constant ξ_0 is an unknown coupling constant describing these transitions. Note, using the same ξ_0 in front of both terms means that the Lagrangian \mathcal{L}_{DD^*} fulfills isospin symmetry. The resulting energy dependent coupling of $\chi_{c1}(2P)$ to $\psi(1S)\rho$ is proportional to

$$\xi_{\chi_{c1}(2P) \rightarrow \psi(1S)\rho}(m) = \xi_0 g_{\chi_{c1} DD^*} [\Sigma_{D^{*0}\bar{D}^0+h.c.}(s) - \Sigma_{D^{*+}D^-+h.c.}(s)] , \quad (37)$$

while the coupling to $\psi(1S)\omega$ to

$$\xi_{\chi_{c1}(2P) \rightarrow \psi(1S)\omega}(m) = \xi_0 g_{\chi_{c1} DD^*} [\Sigma_{D^{*0}\bar{D}^0+h.c.}(s) + \Sigma_{D^{*+}D^-+h.c.}(s)] + \lambda_{gg} \quad (38)$$

with $s = m^2$. Note, in the latter case the two-gluon contribution mentioned previously has been formally included into the parameter λ_{gg} .

The real part of the loops is depicted in Fig. 5. Equation (37) is not exactly zero because the loops $\Sigma_{D^{*0}\bar{D}^0+h.c.}(s)$ and $\Sigma_{D^{*+}D^-+h.c.}(s)$ differ, due to the small mass difference between the neutral and charged mesons D and D^* (in turn, caused by the small mass difference between the quarks u and d). Nevertheless, when s is far from the $D^{*0}D^0$ and $D^{*+}D^-$ thresholds, the difference between the loops in Eq. (37) is very small (see Fig. 5). At the mass of the state coming from the seed in case I, i.e. 3.99 GeV, the coupling to $\psi(1S)\rho$ (Eq. (37)) can be safely neglected. On the contrary, as shown in Fig. 5, for the mass of the $X(3872)$ the situation is different: the difference between the $D^{*0}D^0$ and the $D^{*+}D^-$ loops is non-negligible and quite important.

In what concerns the coupling $\xi_{\chi_{c1}(2P) \rightarrow \psi(1S)\omega}$ in Eq. (38), the sum of the loops ensures that it is large for both the $X(3872)$ and the seed state. Here, as a first approximation, we shall neglect the direct two-gluon contribution λ_{gg} , since close to DD^* thresholds the loops are large (the real parts have a peak in that energy region, see Fig. 5), and the coupling constant $g_{\chi_{c1} DD^*}$ is sizable (see also the recent argument in Ref. [38]). At $m = 3.872$ GeV, corresponding to the $X(3872)$, one has the following ratio:

$$\left| \frac{\xi_{\chi_{c1}(2P) \rightarrow \psi(1S)\omega}(m)}{\xi_{\chi_{c1}(2P) \rightarrow \psi(1S)\rho}(m)} \right|_{m=3.872 \text{ GeV}}^2 \simeq \left| \frac{\Sigma_{D^{*0}\bar{D}^0+h.c.}(s) + \Sigma_{D^{*+}D^-+h.c.}(s)}{\Sigma_{D^{*0}\bar{D}^0+h.c.}(s) - \Sigma_{D^{*+}D^-+h.c.}(s)} \right|_{s=3.872 \text{ GeV}^2}^2 = 12.3 . \quad (39)$$

Thus, the coupling $\xi_{\chi_{c1}(2P) \rightarrow \psi(1S)\rho}$ is indeed non-negligible (even if, as expected, suppressed). On the other hand, for $m = 3.986$ GeV (at the broad seed peak) one finds a ratio of about 630, thus showing that the decay to $\psi(1S)\rho$ is heavily suppressed (the loops cancel to a very good extent). Thus, for the seed state at about 3.986 GeV there is only the decay into $\psi(1S)\omega$.

The decay widths of $\chi_{c1}(2P)$, with a running mass m , into ω (or ρ), with a running mass x , can be summarized as:

$$\Gamma_{\chi_{c1}(2P) \rightarrow \psi(1S)\omega}(m, x) = \xi_{\chi_{c1}(2P) \rightarrow \psi(1S)\omega}^2 V(m, x) , \quad (40)$$

$$\Gamma_{\chi_{c1}(2P) \rightarrow \psi(1S)\rho}(m, x) = \xi_{\chi_{c1}(2P) \rightarrow \psi(1S)\rho}^2 V(m, x) , \quad (41)$$

with

$$V(m, x) = \frac{k}{8\pi m^2} \frac{1}{3m_{\psi(1S)}^2} \left[4k^4 + 6m_{\psi(1S)}^2 x^2 + 2k^2 \left(2m_{\psi(1S)}^2 + x^2 + 2\sqrt{k^2 + m_{\psi(1S)}^2} \sqrt{k^2 + x^2} \right) \right], \quad (42)$$

where $k = k(m, m_{\psi(1S)}, x)$. Then, by fixing the mass to $m = 3.872$ GeV, and further integrating over the ρ mass, the decay $X(3872) \rightarrow \psi(1S)\rho^0 \rightarrow \psi(1S)\pi^+\pi^-$ reads:

$$\Gamma_{X(3872) \rightarrow \psi(1S)\pi^+\pi^-} = \left| \xi_{\chi_{c1}(2P) \rightarrow \psi(1S)\rho}(m_{X(3872)}) \right|^2 \int_0^\infty dx V(m_{X(3872)}, x) d_\rho(x), \quad (43)$$

where $d_\rho(x)$ is the spectral function of the ρ meson. Here, we shall use a relativistic Breit-Wigner function:

$$d_{\rho^0}(x) = N_\rho \frac{\theta(x - 2m_{\pi^+})}{(x^2 - m_{\rho^0}^2)^2 + \Gamma_{\rho^0}^2 m_{\rho^0}^2}, \quad (44)$$

with the parameters $m_{\rho^0} = 775.26 \pm 0.25$ MeV, $\Gamma_{\rho^0} = 147.8 \pm 0.9$ MeV, and N_ρ such that $\int_0^\infty dx d_\rho(x) = 1$.

Similarly, the decay $X(3872) \rightarrow \psi(1S)\omega \rightarrow \psi(1S)\pi^+\pi^-\pi^0$ is obtained upon integrating over the ω mass:

$$\Gamma_{X(3872) \rightarrow \psi(1S)\pi^+\pi^-\pi^0} = \left| \xi_{\chi_{c1}(2P) \rightarrow \psi(1S)\omega}(m_{X(3872)}) \right|^2 \int_0^\infty dx V(m_{X(3872)}, x) d_\omega(x), \quad (45)$$

where

$$d_\omega(x) = N_\omega \frac{\theta(x - 2m_{\pi^+} - m_{\pi^0})}{(x^2 - m_\omega^2)^2 + \Gamma_\omega^2 m_\omega^2}, \quad (46)$$

with $m_\omega = 782.65 \pm 0.12$ MeV, $\Gamma_\omega = 8.49 \pm 0.08$ MeV, and N_ω such that $\int_0^\infty dx d_\omega(x) = 1$.

Finally, the following ratio is obtained:

$$\frac{\Gamma_{X(3872) \rightarrow \psi(1S)\pi^+\pi^-\pi^0}}{\Gamma_{X(3872) \rightarrow \psi(1S)\pi^+\pi^-}} \simeq 1.9 \quad (47)$$

which is comparable with the experimental value 0.8 ± 0.3 .

In conclusion, the originally small isospin breaking coupling to $J/\psi\rho$ is enhanced at the mass of the $X(3872)$, due to the difference between the real parts of the neutral and charged loops. In this way, a qualitative agreement with data is obtained. This is a surprisingly good result obtained without any further assumptions and free parameters.

Improvements are possible: the phenomenological Lagrangian of Eq. (36), that describes the transition DD^* into $J/\psi\omega$ and $J/\psi\rho$, is a useful but still rather simple approximation. Moreover, the small but nonzero role of the direct two-gluon process, parametrized by λ_{gg} in Eq. (38), can slightly change the result (for instance, a small destructive interference would decrease the coupling into the $J/\psi\omega$ channel). A better spectral function of the ρ -meson, which goes beyond the relativistic Breit-Wigner approximation of Eq. (44), would also lead to a smaller ratio due to the fact that a greater weight appears at lower energies once a form factor for the ρ is taken into account. Yet, such a procedure would imply the need of additional parameters and would only lead to small changes, therefore it is not considered in this work. Finally, the ratio in Eq. (47) is reported for different values in the Appendix A.

IV. CONCLUSIONS

The state $X(3872)$ shows some features compatible with a $\bar{c}c$ state, such as radiative decays and prompt production, and other features compatible with a $D^0 D^{*0}$ molecular state, such as the mass close to the $D^0 D^{*0}$ threshold and an isospin-breaking decay into $J/\psi\rho$.

In this paper we have shown that both aspects are naturally described within a simple approach. Our Lagrangian contains initially a single $\bar{c}c$ state, dressed by mesonic DD^* loops. In the complex plane, one finds two poles: a standard seed pole in the III RS corresponding to the predominantly $\bar{c}c$ object $\chi_{c1}(2P)$, with a total strong decay width of about 80 MeV (in agreement with the predictions of the quark model), and, in addition, a virtual pole on the

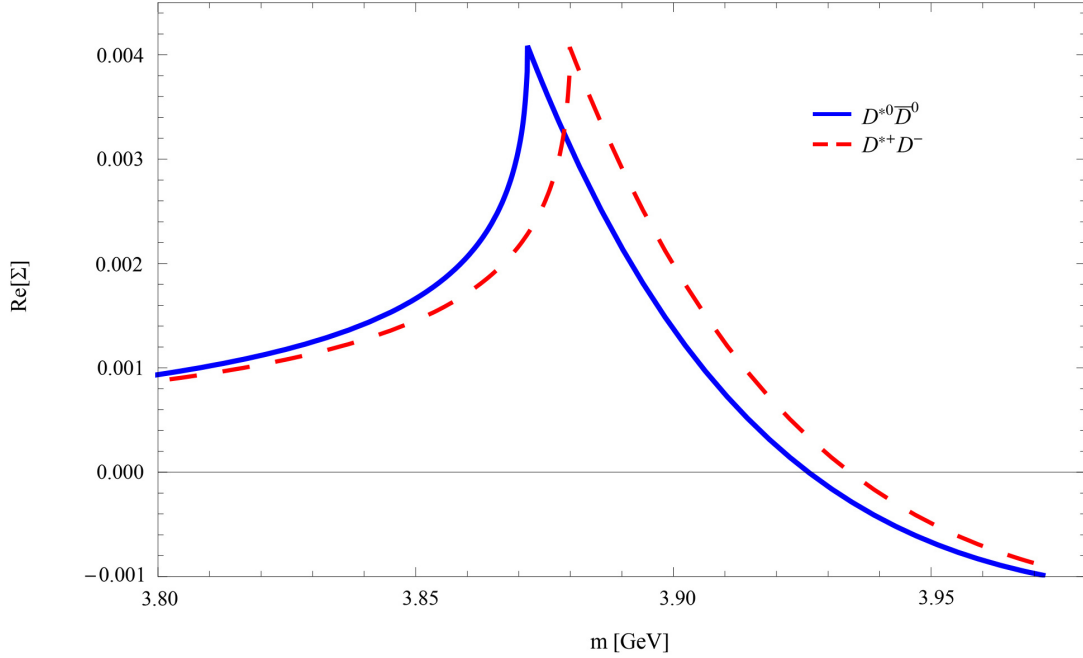


FIG. 5: Real part of the loop functions $\Sigma_{D^0 D^{*0}}(m^2)$ and $\Sigma_{D^+ D^{*-}}(m^2)$, see Eq. (6). The peaks at the thresholds are a salient features of these objects. The difference between them in the energy region close to the thresholds is visible: this is in the end responsible for the isospin suppressed decay into $J/\psi\rho$.

II RS just below $D^0 D^{*0}$ threshold is developed, responsible for the high peak of the spectral function at threshold, identified with $X(3872)$.

The overall spectral function, correctly normalized to unity, describes simultaneously the state coming from the seed, i.e., the $\chi_{c1}(2P)$, and the $X(3872)$. The $\bar{c}c$ seed state corresponds to a large bump on the right side of the spectral function, but for some parameter choices the bump disappears, eventually explaining why this state was not yet measured. Moreover, the $X(3872)$ emerges automatically as a mixed object. Strong and radiative decays and prompt production depend on the $\bar{c}c$ core, while the decays into $J/\psi\rho$ and $J/\psi\omega$ are strongly affected by the $D^0 D^{*0}$ and $D^+ D^{*-}$ loops. Even if some molecular properties appear, the understanding of the $X(3872)$ is quite different from a standard nonrelativistic molecule. The very existence of the $X(3872)$ is due to the nearby quarkonium state.

Besides the understanding of the puzzling properties of the $X(3872)$, we have also made predictions for the strong decay to $D^0 D^{*0}$, for the radiative decays to $\psi(1S)\gamma$ and $\psi(2S)\gamma$, and for the ratio between the decays to $J/\psi\rho$ and $J/\psi\omega$.

In conclusion, the $X(3872)$ emerges from a very peculiar interplay between a quark-antiquark axial-vector state, and the thresholds placed at a critical distance. It is then not surprising that no analogous state has been found in the bottomonium sector [62–65]. In fact, the existence of the $X(3872)$, as part of the spectral function of the $\chi_{c1}(2P)$, emerges from the fulfillment of specific conditions, most notably the proper distance to the relevant thresholds and the corresponding couplings. Going from the charm to the bottomonium sector is likely to ruin these somewhat delicate conditions at least for the analogous system, since the bottomonium states are typically more bound than the charmonium ones, and the second and third radial excitations of the axial-vector bottomonium are unlikely to be close enough to their respective s -wave BB^* decay channel. Yet, it is possible that other states analogous to the $X(3872)$ emerge in other parts of the rich QCD spectrum.

Acknowledgements F.G. thanks A. Pilloni for useful discussions. The authors acknowledge financial support from the Polish National Science Centre (NCN) through the OPUS project no. 2015/17/B/ST2/01625.

Appendix A: Results for parameter variation

In this appendix we check how the results of our model vary upon changing the free parameters. In Tables I–VIII, we report the main outcomes of our approach. For each case tested here we show the numerical values of the following

quantities: the coupling constant $g_{\chi_{c1}DD^*}$; the probability that the dressed state $\chi_{c1}(2P)$ is contained between the left threshold and 1 MeV above it, see Eq. (15); the decay width into $D^{*0}\bar{D}^0$, see Eq. (21); the pole positions in the complex energy plane; the radiative decays reported in Eqs. (34) and (35); the ratio of Eq. (47) involving the isospin-breaking decay into $J/\psi\rho^0$.

1. Variation of $g_{\chi_{c1}DD^*}$ at fixed Λ , tested for two types of form factors

As a first step, for the fixed cutoff value $\Lambda = 0.5$ GeV, we test different values of the coupling constant $g_{\chi_{c1}DD^*}$, obtained by changing the mass m_* , defined in Eq. (13), in the range between $D^{*0}D^0$ and $D^{*+}D^-$ thresholds. The critical value of $g_{\chi_{c1}DD^*}$ corresponds to the case when m_* sits just at the $D^{*0}D^0$ threshold (thus, the virtual pole has a mass just below $m_{D_0} + m_{D_0^*}$, if the coupling is infinitesimally smaller than the critical value). Moreover, we also study one case in which m_* lies below $D^{*0}D^0$: here, there is a real bound state and the spectral function has the form given by Eq. (22).

In what concerns the bare mass of the charmonium, we use the two values employed for the cases I and II described in the text, viz. $m_0 = 3.95$ GeV [9] in Sec. A 1 a and $m_0 = 3.92$ GeV [11] in Sec. A 1 b.

Moreover, we have repeated all the calculations for two types of form factors, the first one given by the Gaussian function in Eq. (4), while the second one has the form:

$$F_\Lambda \equiv F_\Lambda^{\text{dipolar}}(k) = \left(1 + \frac{k^4}{\Lambda^4}\right)^{-2}. \quad (\text{A1})$$

The variation of the coupling constant $g_{\chi_{c1}DD^*}$, as well as the specific choice of the form factor, either (4) or (A1), does not affect the overall picture, which is quite stable and consistent for the presented results. In each case, there is a strong enhancement close to the $D^{*0}D^0$ threshold and there are two poles in the complex plane, one corresponding to the seed state and one to the $X(3872)$ (which is virtual when the coupling constant is smaller than the critical value, and real otherwise). The pole corresponding to the $X(3872)$ (indicated by \blacklozenge in the tables) is a virtual pole (that is, in the II RS) when $g_{\chi_{c1}DD^*}$ is smaller than a critical value, but a bound-state (on the I RS) when $g_{\chi_{c1}DD^*}$ exceeds the critical value. This is the case for Tables I-IV.

It is interesting to note that the state $X(3872)$ fades away when the coupling constant decreases. This property confirms that the very existence of the $X(3872)$ is due to the nearby quarkonium state. Interestingly, a similar conclusion was achieved in Ref. [26] and [28], where the $X(3872)$ always required a small charmonium component to exist. However, the predictions concerning the $\chi_{c1}(2P)$ diverge from the present approach. In these references, by employing potential models with a harmonic oscillator as a confinement potential, the state that is found between 4.0 and 4.1 GeV is much larger than the pole at 3.99 GeV within the present approach, so that it would hardly be observed in the experiment. On the other hand, either for a seed value of 3.95 GeV, or by the inclusion of additional decay channels, the $X(3872)$ becomes a seed pole, rather than a dynamically generated one. Such possibility should be disentangled by a possible experimental observation of the $\chi_{c1}(2P)$ state, as we present here. Another important difference is that, within the present paper, we can understand radiative and isospin-violating decay of $X(3872)$ without additional assumptions, see Sec. III.

a. $m_0 = 3.95 \text{ GeV}$

The results for $m_0 = 3.95 \text{ GeV}$ are presented in Table I (Gaussian form factor) and Table II (dipolar form factor).

| Gaussian form factor, | | | $\Lambda = 0.5 \text{ GeV},$ | $m_0 = 3.95 \text{ GeV},$ | $m_* \neq \text{const.}$ | |
|------------------------------|----------|-------------------|---|---------------------------|--------------------------|----------|
| $g_{\chi_{c1}DD^*}$ [GeV] | Eq. (15) | Eq. (21) [MeV] | Pole positions [GeV] | Eq. (34) [keV] | Eq. (35) [keV] | Eq. (47) |
| 9.808 (critical) | 0.057 | 0.636 | • $3.9961 - 0.0359 i$ ◆ $3.8717 - i\varepsilon$ | 0.628 | 3.64 | 1.92 |
| 9.732 (case I) | 0.049 | 0.607 | • $3.9954 - 0.0357 i$ ◆ $3.8716 - i\varepsilon$ | 0.539 | 3.13 | 1.92 |
| 9.500 | 0.029 | 0.408 | • $3.9933 - 0.0354 i$ ◆ $3.8715 - i\varepsilon$ | 0.323 | 1.88 | 1.92 |
| 9.300 | 0.019 | 0.263 | • $3.9915 - 0.0350 i$ ◆ $3.8710 - i\varepsilon$ | 0.206 | 1.20 | 1.92 |
| 9.000 | 0.010 | 0.136 | • $3.9887 - 0.0344 i$ ◆ $3.8699 - i\varepsilon$ | 0.110 | 0.64 | 1.92 |
| 8.800 | 0.007 | 0.091 | • $3.9869 - 0.0339 i$ ◆ $3.8689 - i\varepsilon$ | 0.076 | 0.44 | 1.92 |
| 8.000 | 0.002 | 0.024 | • $3.9796 - 0.0316 i$ ◆ $3.8609 - i\varepsilon$ | 0.024 | 0.14 | 1.92 |
| 10.000 | 0.035 | 0.505 | • $3.9978 - 0.0361 i$ ◆ $3.8716 - i\varepsilon \text{ (I RS)}$ | 0.387 | 2.25 | 1.92 |

TABLE I: Results for different values of the coupling constant $g_{\chi_{c1}DD^*}$, calculated for $\Lambda = 0.5 \text{ GeV}$, bare mass $m_0 = 3.95 \text{ GeV}$, and Gaussian vertex function. The symbols (•) and (◆) indicate the seed pole and the virtual companion pole, respectively.

| Dipolar form factor, | | | $\Lambda = 0.5 \text{ GeV},$ | $m_0 = 3.95 \text{ GeV},$ | $m_* \neq \text{const.}$ | |
|------------------------------|----------|-------------------|--|---------------------------|--------------------------|----------|
| $g_{\chi_{c1}DD^*}$ [GeV] | Eq. (15) | Eq. (21) [MeV] | Pole positions [GeV] | Eq. (34) [keV] | Eq. (35) [keV] | Eq. (47) |
| 8.339 (critical) | 0.078 | 0.630 | • $4.0075 - 0.0390 i$ ◆ $3.8717 - i\varepsilon$ | 0.856 | 4.97 | 2.87 |
| 8.179 | 0.047 | 0.481 | • $4.006 - 0.0389 i$ ◆ $3.8715 - i\varepsilon$ | 0.520 | 3.02 | 2.87 |
| 7.800 | 0.013 | 0.138 | • $4.001 - 0.0385 i$ ◆ $3.8675 - i\varepsilon$ | 0.146 | 0.85 | 2.87 |
| 7.500 | 0.060 | 0.059 | • $3.9980 - 0.0381 i$ ◆ $3.8616 - i\varepsilon$ | 0.066 | 0.38 | 2.87 |
| 7.200 | 0.0032 | 0.029 | • $3.9945 - 0.0376 i$ ◆ $3.8628 - i\varepsilon$ | 0.35 | 0.21 | 2.87 |
| 7.000 | 0.0022 | 0.020 | • $3.9921 - 0.0373 i$ ◆ $3.8707 - i\varepsilon$ | 0.025 | 0.15 | 2.87 |
| 6.500 | 0.0011 | 0.008 | • $3.9861 - 0.0361 i$ ◆ $3.8658 - i\varepsilon$ | 0.012 | 0.072 | 2.87 |
| 8.500 | 0.039 | 0.417 | • $4.009 - 0.0391 i$ ◆ $3.8716 - i\varepsilon \text{ (I RS)}$ | 0.426 | 2.48 | 2.87 |

TABLE II: Similar to Table I, but for dipolar form factor.

b. $m_0 = 3.92 \text{ GeV}$

The results for $m_0 = 3.92 \text{ GeV}$ are presented in Table III (Gaussian form factor) and Table IV (dipolar form factor).

| Gaussian form factor, | | | $\Lambda = 0.5 \text{ GeV},$ | $m_0 = 3.92 \text{ GeV},$ | $m_* \neq \text{const.}$ | |
|------------------------------|----------|-------------------|---|---------------------------|--------------------------|----------|
| $g_{\chi_{c1}DD^*}$ [GeV] | Eq. (15) | Eq. (21) [MeV] | Pole positions [GeV] | Eq. (34) [keV] | Eq. (35) [keV] | Eq. (47) |
| 7.689 (critical) | 0.092 | 0.634 | • $3.9547 - 0.0444 i$ ◆ $3.8717 - i\varepsilon$ | 1.02 | 5.91 | 1.92 |
| 7.557 (case II) | 0.067 | 0.544 | • $3.9531 - 0.0440 i$ ◆ $3.8716 - i\varepsilon$ | 0.74 | 4.27 | 1.92 |
| 7.400 | 0.043 | 0.373 | • $3.9513 - 0.0435 i$ ◆ $3.8713 - i\varepsilon$ | 0.48 | 2.77 | 1.92 |
| 7.300 | 0.033 | 0.283 | • $3.9501 - 0.0432 i$ ◆ $3.8710 - i\varepsilon$ | 0.36 | 2.08 | 1.92 |
| 7.000 | 0.015 | 0.123 | • $3.9465 - 0.0420 i$ ◆ $3.8689 - i\varepsilon$ | 0.16 | 0.95 | 1.92 |
| 6.800 | 0.009 | 0.075 | • $3.9441 - 0.0412 i$ ◆ $3.8664 - i\varepsilon$ | 0.10 | 0.60 | 1.92 |
| 6.600 | 0.006 | 0.048 | • $3.9417 - 0.0402 i$ ◆ $3.8629 - i\varepsilon$ | 0.07 | 0.41 | 1.92 |
| 8.000 | 0.034 | 0.340 | • $3.9582 - 0.0452 i$ ◆ $3.8714 - i\varepsilon$ (I RS) | 0.38 | 2.19 | 1.92 |

TABLE III: Results for different values of the coupling constant $g_{\chi_{c1}DD^*}$, calculated for $\Lambda = 0.5 \text{ GeV}$, bare mass $m_0 = 3.92 \text{ GeV}$, and Gaussian vertex function. The symbols (•) and (◆) indicate the seed pole and the virtual companion pole, respectively.

| Dipolar form factor, | | | $\Lambda = 0.5 \text{ GeV},$ | $m_0 = 3.92 \text{ GeV},$ | $m_* \neq \text{const.}$ | |
|------------------------------|----------|-------------------|---|---------------------------|--------------------------|----------|
| $g_{\chi_{c1}DD^*}$ [GeV] | Eq. (15) | Eq. (21) [MeV] | Pole position [GeV] | Eq. (34) [keV] | Eq. (35) [keV] | Eq. (47) |
| 6.537 (critical) | 0.125 | 0.62 | • $3.9700 - 0.0498 i$ ◆ $3.8717 - i\varepsilon$ | 1.38 | 8.00 | 2.87 |
| 6.351 | 0.062 | 0.40 | • $3.9674 - 0.0498 i$ ◆ $3.8712 - i\varepsilon$ | 0.68 | 3.94 | 2.87 |
| 6.000 | 0.015 | 0.094 | • $3.9624 - 0.0498 i$ ◆ $3.8678 - i\varepsilon$ | 0.16 | 0.96 | 2.87 |
| 5.800 | 0.081 | 0.048 | • $3.95934 - 0.0497 i$ ◆ $3.8682 - i\varepsilon$ | 0.09 | 0.52 | 2.87 |
| 5.500 | 0.0039 | 0.021 | • $3.9546 - 0.0495 i$ ◆ $3.8688 - i\varepsilon$ | 0.043 | 0.25 | 2.87 |
| 5.200 | 0.0022 | 0.011 | • $3.9495 - 0.0492 i$ ◆ $3.8694 - i\varepsilon$ | 0.024 | 0.14 | 2.87 |
| 4.500 | 0.0008 | 0.0029 | • $3.9355 - 0.0477 i$ ◆ $3.8960 - i\varepsilon$ | 0.0088 | 0.051 | 2.87 |
| 6.800 | 0.032 | 0.23 | • $3.9735 - 0.0498 i$ ◆ $3.8713 - i\varepsilon$ (I RS) | 0.35 | 2.03 | 2.87 |

TABLE IV: Similar to Table III but for a dipolar form factor.

2. Variation of Λ at fixed m_* , tested for two types of form factors

For completeness, we study the dependence of the results on the parameter Λ . We test different Λ in the range from 0.4 GeV to 0.8 GeV. Similarly to Sec. A 1, we use the two bare masses $m_0 = 3.95$ GeV (Sec. A 2 a) and $m_0 = 3.92$ GeV (Sec. A 2 b), as well as the Gaussian and dipolar form factors. In order to determine the coupling constant $g_{\chi_{c1}DD^*}$, we set $m_* = 3.874$ GeV (in between the two DD^* thresholds, just as done in the main text). One should notice that, even if m_* is fixed, the coupling constant varies.

We conclude that the value of the cutoff in the quite large range from 0.4 GeV to 0.8 GeV does not change the most important features emerging from our approach. For each value of Λ , two poles are observed on the complex energy plane. However, the value $\Lambda = 0.8$ GeV should be regarded as an upper limit, since the imaginary part of the pole corresponding to the standard seed state gives rise to a too large decay width when compared with the predictions of the quark model with a Cornell potential. For $m_0 = 3.95$ GeV, the obtained decay widths are ~ 225 MeV and ~ 292 MeV for Gaussian and dipolar form factors, respectively. Similarly, for $m_0 = 3.92$ GeV we get ~ 217 MeV and ~ 359 MeV for these two form factors. In such cases, the predominantly $\bar{c}c$ would be very difficult to detect in the experiment, but the width would be similar to the one obtained in quark model approaches which employ an harmonic oscillator potential [26].

a. $m_0 = 3.95 \text{ GeV}$

The results for $m_0 = 3.95 \text{ GeV}$ are presented in Table V (Gaussian form factor) and Table VI (dipolar form factor).

| Gaussian form factor, $\Lambda \neq \text{const.}$, $m_0 = 3.95 \text{ GeV}$, $m_* = 3.874 \text{ GeV}$. | | | | | | | |
|--|------------------------------|----------|-------------------|--|-------------------|-------------------|----------|
| Λ [GeV] | $g_{\chi_{c1}DD^*}$ [GeV] | Eq. (15) | Eq. (21) [MeV] | Pole positions [GeV] | Eq. (34) [keV] | Eq. (35) [keV] | Eq. (47) |
| 0.4 | 11.259 | 0.040 | 0.629 | • $3.9861 - 0.0171 i$ ◆ $3.8717 - i\varepsilon$ | 0.444 | 2.57 | 1.32 |
| 0.42 | 10.897 | 0.045 | 0.636 | • $3.9883 - 0.0204 i$ ◆ $3.8717 - i\varepsilon$ | 0.499 | 2.89 | 1.43 |
| 0.45 | 10.413 | 0.048 | 0.632 | • $3.9913 - 0.0258 i$ ◆ $3.8717 - i\varepsilon$ | 0.528 | 3.07 | 1.61 |
| 0.5 | 9.732 (case I) | 0.049 | 0.607 | • $3.9954 - 0.0357 i$ ◆ $3.8716 - i\varepsilon$ | 0.539 | 3.13 | 1.92 |
| 0.55 | 9.169 | 0.050 | 0.577 | • $3.9983 - 0.0468 i$ ◆ $3.8716 - i\varepsilon$ | 0.551 | 3.20 | 2.27 |
| 0.6 | 8.694 | 0.051 | 0.549 | • $3.9998 - 0.0588 i$ ◆ $3.8716 - i\varepsilon$ | 0.562 | 3.26 | 2.65 |
| 0.7 | 7.930 | 0.053 | 0.497 | • $3.9983 - 0.0848 i$ ◆ $3.8715 - i\varepsilon$ | 0.582 | 3.38 | 3.49 |
| 0.8 | 7.338 | 0.054 | 0.454 | • $3.9899 - 0.1123 i$ ◆ $3.8715 - i\varepsilon$ | 0.600 | 3.49 | 4.45 |

TABLE V: Results for different values of cutoff Λ . The used parameters are: bare mass $m_0 = 3.95 \text{ GeV}$, $m_* = 3.874 \text{ GeV}$ and a Gaussian vertex function. The symbols (•) and (◆) indicate the seed pole and the virtual companion pole, respectively.

| Dipolar form factor, $\Lambda \neq \text{const.}$, $m_0 = 3.95 \text{ GeV}$, $m_* = 3.874 \text{ GeV}$. | | | | | | | |
|---|------------------------------|----------|-------------------|--|-------------------|-------------------|----------|
| Λ [GeV] | $g_{\chi_{c1}DD^*}$ [GeV] | Eq. (15) | Eq. (21) [MeV] | Pole positions [GeV] | Eq. (34) [keV] | Eq. (35) [keV] | Eq. (47) |
| 0.4 | 9.369 | 0.0440 | 0.552 | • $3.9909 - 0.0192 i$ ◆ $3.8716 - i\varepsilon$ | 0.485 | 2.82 | 1.90 |
| 0.42 | 9.090 | 0.0447 | 0.536 | • $3.9939 - 0.0226 i$ ◆ $3.8716 - i\varepsilon$ | 0.493 | 2.86 | 2.08 |
| 0.45 | 8.714 | 0.0457 | 0.514 | • $3.9984 - 0.0282 i$ ◆ $3.8716 - i\varepsilon$ | 0.503 | 2.92 | 2.36 |
| 0.5 | 8.179 | 0.0472 | 0.481 | • $4.0057 - 0.0389 i$ ◆ $3.8715 - i\varepsilon$ | 0.520 | 3.02 | 2.87 |
| 0.55 | 7.732 | 0.0486 | 0.452 | • $4.0126 - 0.0515 i$ ◆ $3.8714 - i\varepsilon$ | 0.536 | 3.12 | 3.43 |
| 0.6 | 7.351 | 0.0499 | 0.427 | • $4.0190 - 0.0660 i$ ◆ $3.8714 - i\varepsilon$ | 0.550 | 3.20 | 4.04 |
| 0.7 | 6.732 | 0.0522 | 0.384 | • $4.0298 - 0.1013 i$ ◆ $3.8711 - i\varepsilon$ | 0.575 | 3.34 | 5.42 |
| 0.8 | 6.249 | 0.0539 | 0.348 | • $4.0376 - 0.1458 i$ ◆ $3.8706 - i\varepsilon$ | 0.595 | 3.46 | 7.00 |

TABLE VI: Similar to Table V but for a dipolar vertex function.

b. $m_0 = 3.92 \text{ GeV}$

The results for $m_0 = 3.92 \text{ GeV}$ are presented in Tables VII (Gaussian form factor), and VIII (dipolar form factor).

| Gaussian form factor, $\Lambda \neq \text{const.}$, $m_0 = 3.92 \text{ GeV}$, $m_* = 3.874 \text{ GeV}$. | | | | | | | |
|--|------------------------------|----------|-------------------|--|-------------------|-------------------|----------|
| Λ [GeV] | $g_{\chi_{c1}DD^*}$ [GeV] | Eq. (15) | Eq. (21) [MeV] | Pole positions [GeV] | Eq. (34) [keV] | Eq. (35) [keV] | Eq. (47) |
| 0.4 | 8.743 | 0.0662 | 0.626 | • $3.9507 - 0.0246 i$ ♦ $3.8717 - i\varepsilon$ | 0.729 | 4.23 | 1.32 |
| 0.42 | 8.461 | 0.0663 | 0.612 | • $3.9517 - 0.0282 i$ ♦ $3.8717 - i\varepsilon$ | 0.730 | 4.24 | 1.43 |
| 0.45 | 8.086 | 0.0664 | 0.587 | • $3.9527 - 0.0339 i$ ♦ $3.8716 - i\varepsilon$ | 0.732 | 4.25 | 1.61 |
| 0.5 (case II) | 7.557 | 0.0667 | 0.544 | • $3.9531 - 0.0440 i$ ♦ $3.8716 - i\varepsilon$ | 0.735 | 4.27 | 1.92 |
| 0.55 | 7.120 | 0.0670 | 0.504 | • $3.9519 - 0.0548 i$ ♦ $3.8716 - i\varepsilon$ | 0.738 | 4.29 | 2.27 |
| 0.6 | 6.751 | 0.0672 | 0.468 | • $3.9490 - 0.0659 i$ ♦ $3.8715 - i\varepsilon$ | 0.741 | 4.31 | 2.65 |
| 0.7 | 6.157 | 0.0675 | 0.408 | • $3.9373 - 0.0883 i$ ♦ $3.8713 - i\varepsilon$ | 0.744 | 4.33 | 3.49 |
| 0.8 | 5.698 | 0.0674 | 0.359 | • $3.9172 - 0.1087 i$ ♦ $3.8708 - i\varepsilon$ | 0.744 | 4.33 | 4.45 |

TABLE VII: Results for different values of cutoff Λ . The used parameters are: bare mass $m_0 = 3.92 \text{ GeV}$, $m_* = 3.874 \text{ GeV}$, and a Gaussian vertex function. The symbols (•) and (♦) indicate the seed pole and the virtual companion pole, respectively.

| Dipolar form factor, $\Lambda \neq \text{const.}$, $m_0 = 3.92 \text{ GeV}$, $m_* = 3.874 \text{ GeV}$. | | | | | | | |
|---|------------------------------|----------|-------------------|--|-------------------|-------------------|----------|
| Λ [GeV] | $g_{\chi_{c1}DD^*}$ [GeV] | Eq. (15) | Eq. (21) [MeV] | Pole positions [GeV] | Eq. (34) [keV] | Eq. (35) [keV] | Eq. (47) |
| 0.4 | 7.275 | 0.060 | 0.483 | • $3.9572 - 0.0265 i$ ♦ $3.8715 - i\varepsilon$ | 0.660 | 3.84 | 1.90 |
| 0.42 | 7.058 | 0.060 | 0.463 | • $3.9594 - 0.0305 i$ ♦ $3.8715 - i\varepsilon$ | 0.664 | 3.86 | 2.08 |
| 0.45 | 6.766 | 0.061 | 0.437 | • $3.9626 - 0.0371 i$ ♦ $3.8714 - i\varepsilon$ | 0.670 | 3.90 | 2.36 |
| 0.5 | 6.351 | 0.062 | 0.399 | • $3.9674 - 0.0498 i$ ♦ $3.8712 - i\varepsilon$ | 0.678 | 3.94 | 2.87 |
| 0.55 | 6.004 | 0.062 | 0.366 | • $3.9715 - 0.0647 i$ ♦ $3.8709 - i\varepsilon$ | 0.684 | 3.98 | 3.43 |
| 0.6 | 5.708 | 0.062 | 0.338 | • $3.9748 - 0.0819 i$ ♦ $3.8703 - i\varepsilon$ | 0.688 | 4.00 | 4.04 |
| 0.7 | 5.228 | 0.0632 | 0.291 | • $3.9790 - 0.1244 i$ ♦ $3.8698 - i\varepsilon$ | 0.692 | 4.03 | 5.42 |
| 0.8 | 4.852 | 0.063 | 0.254 | • $3.9813 - 0.1793 i$ ♦ $3.8704 - i\varepsilon$ | 0.690 | 4.01 | 7.00 |

TABLE VIII: Similar to Table VII but for a dipolar vertex function.

-
- [1] S.K. Choi *et al.* (Belle Collaboration), *Observation of a narrow charmonium-like state in exclusive $B^\pm \rightarrow K^\pm \pi^+ \pi^- J/\psi$ decays*, Phys. Rev. Lett. **91**, 262001 (2003).
- [2] M. Tanabashi *et al.* (Particle Data Group), Phys. Rev. D **98**, 030001 (2018).
- [3] H.X. Chen, W. Chen, X. Liu, and S.L. Zhu, *The hidden-charm pentaquark and tetraquark states*, Phys. Rept. **639**, 1 (2016).
- [4] N. Brambilla *et al.*, *Heavy quarkonium: progress, puzzles, and opportunities*, Eur. Phys. J. C **71**, 1534 (2011).
- [5] A. Esposito, A.L. Guerrieri, F. Piccinini, A. Pilloni, and A.D. Polosa, *Four-Quark Hadrons: an Updated Review*, Int. J. Mod. Phys. A **30**, 1530002 (2015).
- [6] M. Nielsen, F.S. Navarra, and S.H. Lee, *New Charmonium States in QCD Sum Rules: A Concise Review*, Phys. Rept. **497**, 41 (2010).
- [7] A. Ali, J.S. Lange, and S. Stone, *Exotics: Heavy Pentaquarks and Tetraquarks*, Prog. Part. Nucl. Phys. **97**, 123 (2017).
- [8] S.L. Olsen, T. Skwarnicki, and D. Zieminska, *Nonstandard heavy mesons and baryons: Experimental evidence*, Rev. Mod. Phys. **90**, 015003 (2018).
- [9] S. Godfrey and N. Isgur, *Mesons in a Relativized Quark Model with Chromodynamics*, Phys. Rev. D **32**, 189 (1985).
- [10] E. Eichten, K. Gottfried, T. Kinoshita, K.D. Lane, and T.M. Yan, *Charmonium: The Model*, Phys. Rev. D **17**, 3090 (1978), Erratum: Phys. Rev. D **21**, 313 (1980); E. Eichten, K. Gottfried, T. Kinoshita, K.D. Lane, and T.M. Yan, *Charmonium: Comparison with Experiment*, Phys. Rev. D **21**, 203 (1980); E. Eichten, K. Gottfried, T. Kinoshita, K. D. Lane and T. M. Yan, *The Interplay of Confinement and Decay in the Spectrum of Charmonium*, Phys. Rev. Lett. **36**, 500 (1976).
- [11] D. Ebert, R.N. Faustov, and V.O. Galkin, *Spectroscopy and Regge trajectories of heavy quarkonia and B_c mesons*, Eur. Phys. J. C **71**, 1825 (2011).
- [12] Y.S. Kalashnikova and A.V. Nefediev, *$X(3872)$ in the molecular model*, arXiv:1811.01324 [hep-ph].
- [13] Y.B. Dong, A. Faessler, T. Gutsche, and V.E. Lyubovitskij, *Estimate for the $X(3872) \rightarrow \gamma J/\psi$ decay width*, Phys. Rev. D **77**, 094013 (2008); Y. Dong, A. Faessler, T. Gutsche, S. Kovalenko, and V.E. Lyubovitskij, *$X(3872)$ as a hadronic molecule and its decays to charmonium states and pions*, Phys. Rev. D **79**, 094013 (2009); Y. Dong, A. Faessler, T. Gutsche, and V. E. Lyubovitskij, *$J/\psi\gamma$ and $\psi(2S)\gamma$ decay modes of the $X(3872)$* , J. Phys. G **38**, 015001 (2011).
- [14] D. Gamermann, J. Nieves, E. Oset, and E. Ruiz Arriola, *Couplings in coupled channels versus wave functions: application to the $X(3872)$ resonance*, Phys. Rev. D **81**, 014029 (2010).
- [15] E. Braaten and J. Stapleton, *Analysis of $J/\psi\pi^+\pi^-$ and $D^0\bar{D}^0\pi^0$ Decays of the $X(3872)$* , Phys. Rev. D **81**, 014019 (2010).
- [16] C. Hanhart, Y.S. Kalashnikova, A.E. Kudryavtsev, and A.V. Nefediev, *Reconciling the $X(3872)$ with the near-threshold enhancement in the $D^0\bar{D}^{*0}$ final state*, Phys. Rev. D **76**, 034007 (2007); F.K. Guo, C. Hanhart, Y.S. Kalashnikova, U.G. Meißner, and A.V. Nefediev, *What can radiative decays of the $X(3872)$ teach us about its nature?*, Phys. Lett. B **742**, 394 (2015).
- [17] T. Barnes and S. Godfrey, *Charmonium options for the $X(3872)$* , Phys. Rev. D **69**, 054008 (2004).
- [18] N.N. Achasov and E.V. Rogozina, *$X(3872)$, $I^G(J^{PC}) = 0^+(1^{++})$, as the $\chi_{1c}(2P)$ charmonium*, Mod. Phys. Lett. A **30**, 1550181 (2015); N.N. Achasov and E.V. Rogozina, *Towards the nature of $X(3872)$ resonance*, J. Univ. Sci. Tech. China **46**, 574 (2016).
- [19] E.J. Eichten, K. Lane, and C. Quigg, *Charmonium levels near threshold and the narrow state $X(3872) \rightarrow \pi^+\pi^- J/\psi$* , Phys. Rev. D **69**, 094019 (2004).
- [20] C. Bignamini, B. Grinstein, F. Piccinini, A.D. Polosa, and C. Sabelli, *Is the $X(3872)$ Production Cross Section at Tevatron Compatible with a Hadron Molecule Interpretation?*, Phys. Rev. Lett. **103**, 162001 (2009).
- [21] A. Esposito, A.L. Guerrieri, L. Maiani, F. Piccinini, A. Pilloni, A.D. Polosa, and V. Riquer, *Observation of light nuclei at ALICE and the $X(3872)$ conundrum*, Phys. Rev. D **92**, 034028 (2015).
- [22] M. Albaladejo, F.K. Guo, C. Hanhart, U.G. Meißner, J. Nieves, A. Nogga, and Z. Yang, *Note on $X(3872)$ production at hadron colliders and its molecular structure*, Chin. Phys. C **41**, 121001 (2017).
- [23] M. Aaboud *et al.* (ATLAS Collaboration), *Measurements of $\psi(2S)$ and $X(3872) \rightarrow J/\psi\pi^+\pi^-$ production in pp collisions at $\sqrt{s} = 8$ TeV with the ATLAS detector*, JHEP **1701**, 117 (2017).
- [24] A. Esposito, B. Grinstein, L. Maiani, F. Piccinini, A. Pilloni, A.D. Polosa, and V. Riquer, *Comment on ‘Note on $X(3872)$ production at hadron colliders and its molecular structure’*, Chin. Phys. C **42**, 114107 (2018).
- [25] P.G. Ortega, J. Segovia, D. R. Entem, and F. Fernandez, *Coupled channel approach to the structure of the $X(3872)$* , Phys. Rev. D **81**, 054023 (2010).
- [26] S. Coito, G. Rupp, and E. van Beveren, *$X(3872)$ is not a true molecule*, Eur. Phys. J. C **73**, 2351 (2013); *Delicate interplay between the $D^0\bar{D}^{*0}$, $\rho^0 J/\psi$, and $\omega J/\psi$ channels in the $X(3872)$ resonance*, Eur. Phys. J. C **71**, 1762 (2011).
- [27] J. Ferretti, G. Galatf, and E. Santopinto, *Interpretation of the $X(3872)$ as a charmonium state plus an extra component due to the coupling to the meson-meson continuum*, Phys. Rev. C **88**, 015207 (2013); J. Ferretti, G. Galatf, and E. Santopinto, *Quark structure of the $X(3872)$ and $\chi_b(3P)$ resonances*, Phys. Rev. D **90**, 054010 (2014).
- [28] M. Cardoso, G. Rupp, and E. van Beveren, *Unquenched quark-model calculation of $X(3872)$ electromagnetic decays*, Eur. Phys. J. C **75**, 26 (2015).
- [29] S. Takeuchi, K. Shimizu, and M. Takizawa, *On the origin of the narrow peak and the isospin symmetry breaking of the $X(3872)$* , PTEP **2014**, 123D01 (2014), Erratum: PTEP **2015**, 079203 (2015).
- [30] L. Maiani, F. Piccinini, A.D. Polosa and V. Riquer, *Diquark-antidiquarks with hidden or open charm and the nature of $X(3872)$* , Phys. Rev. D **71**, 014028 (2005).

- [31] M. Boglione and M.R. Pennington, *Dynamical generation of scalar mesons*, Phys. Rev. D **65**, 114010 (2002).
- [32] M. Boglione and M.R. Pennington, *Unquenching the scalar glueball*, Phys. Rev. Lett. **79**, 1998 (1997).
- [33] N.A. Tornqvist, *Understanding the scalar meson $q\bar{q}$ nonet*, Z. Phys. C **68**, 647 (1995).
- [34] E. van Beveren, T.A. Rijken, K. Metzger, C. Dullemond, G. Rupp, and J.E. Ribeiro, *A Low Lying Scalar Meson Nonet in a Unitarized Meson Model*, Z. Phys. C **30**, 615 (1986).
- [35] T. Wolkanowski, F. Giacosa, and D.H. Rischke, *$a_0(980)$ revisited*, Phys. Rev. D **93**, 014002 (2016).
- [36] T. Wolkanowski, M. Soltysiak, and F. Giacosa, *$K_0^*(800)$ as a companion pole of $K_0^*(1430)$* , Nucl. Phys. B **909**, 418 (2016).
- [37] S. Coito and F. Giacosa, *Line-shape and poles of the $\psi(3770)$* , Nucl. Phys. A **981**, 38 (2019).
- [38] M. Piotrowska, F. Giacosa, and P. Kovacs, *Can the $\psi(4040)$ explain the peak associated with $Y(4008)$?*, Eur. Phys. J. C **79**, 98 (2019).
- [39] J. Terning, *Gauging nonlocal Lagrangians*, Phys. Rev. D **44**, 887 (1991); G. V. Efimov and M. A. Ivanov, *The Quark confinement model of hadrons*, New York, U.S.A., CRC Press, 1993; Y.V. Burdanov, G.V. Efimov, S.N. Nedelko, and S.A. Solunin, *Meson masses within the model of induced nonlocal quark currents*, Phys. Rev. D **54**, 4483 (1996); A. Faessler, T. Gutsche, M. A. Ivanov, V. E. Lyubovitskij, and P. Wang, *Pion and sigma meson properties in a relativistic quark model*, Phys. Rev. D **68**, 014011 (2003); F. Giacosa, T. Gutsche, and A. Faessler, *A Covariant constituent quark-gluon model for the glueball-quarkonia content of scalar-isoscalar mesons*, Phys. Rev. C **71**, 025202 (2005).
- [40] J. Segovia, D. R. Entem, and F. Fernández, *Scaling of the 3P_0 Strength in Heavy Meson Strong Decays*, Phys. Lett. B **715**, 322 (2012).
- [41] P.G. Ortega, J. Segovia, D.R. Entem and F. Fernández, *Charmonium resonances in the $3.9 \text{ GeV}/c^2$ energy region and the $X(3915)/X(3930)$ puzzle*, Phys. Lett. B **778**, 1 (2018).
- [42] J. Segovia, D.R. Entem, F. Fernandez, and E. Hernandez, *Constituent quark model description of charmonium phenomenology*, Int. J. Mod. Phys. E **22**, 1330026 (2013).
- [43] C. Amsler and F. E. Close, *Is $f_0(1500)$ a scalar glueball?*, Phys. Rev. D **53**, 295 (1996).
- [44] E.S. Ackleh, T. Barnes, and E.S. Swanson, *On the mechanism of open flavor strong decays*, Phys. Rev. D **54**, 6811 (1996).
- [45] Z.G. Luo, X.L. Chen, and X. Liu, *$B_{s1}(5830)$ and $B_{s2}^*(5840)$* , Phys. Rev. D **79**, 074020 (2009).
- [46] F. Giacosa and G. Pagliara, *On the spectral functions of scalar mesons*, Phys. Rev. C **76**, 065204 (2007).
- [47] M. Soltysiak and F. Giacosa, *A covariant nonlocal Lagrangian for the description of the scalar kaonic sector*, Acta Phys. Polon. Supp. **9**, 467 (2016).
- [48] J. Schneitzler, T. Wolkanowski, and F. Giacosa, *The role of the next-to-leading order triangle-shaped diagram in two-body hadronic decays*, Nucl. Phys. B **888**, 287 (2014).
- [49] F. Giacosa, *Non-exponential decay in quantum field theory and in quantum mechanics: the case of two (or more) decay channels*, Found. Phys. **42**, 1262 (2012).
- [50] F. Giacosa and G. Pagliara, *Spectral function of a scalar boson coupled to fermions*, Phys. Rev. D **88**, 025010 (2013).
- [51] P. T. Matthews and A. Salam, *Relativistic theory of unstable particles. II*, Phys. Rev. **115**, 1079 (1959).
- [52] E. Braaten and M. Lu, *Line shapes of the $X(3872)$* , Phys. Rev. D **76**, 094028 (2007).
- [53] R. Aaij *et al.* (LHCb Collaboration), *Evidence for the decay $X(3872) \rightarrow \psi(2S)\gamma$* , Nucl. Phys. B **886**, 665 (2014).
- [54] B. Aubert *et al.* (BaBar Collaboration), *Evidence for $X(3872) \rightarrow \psi(2S)\gamma$ in $B^\pm \rightarrow X(3872)K^\pm$ decays, and a study of $B \rightarrow c\bar{c}\gamma K$* , Phys. Rev. Lett. **102**, 132001 (2009).
- [55] A.M. Badalian, V.D. Orlovsky, Y.A. Simonov, and B.L.G. Bakker, *The ratio of decay widths of $X(3872)$ to $\psi'\gamma$ and $J/\psi\gamma$ as a test of the $X(3872)$ dynamical structure*, Phys. Rev. D **85**, 114002 (2012).
- [56] F. K. Guo, C. Hanhart, Y.S. Kalashnikova, U.G. Meißner, and A.V. Nefediev, *What can radiative decays of the $X(3872)$ teach us about its nature?*, Phys. Lett. B **742**, 394 (2015).
- [57] W. Broniowski, F. Giacosa and V. Begun, *Cancellation of the σ meson in thermal models*, Phys. Rev. C **92**, 034905 (2015).
- [58] P.G. Ortega, D.R. Entem, F. Fernandez and E. Ruiz Arriola, *Counting states and the Hadron Resonance Gas: Does $X(3872)$ count?*, Phys. Lett. B **781**, 678 (2018).
- [59] S. Bazak and S. Mrowczynski, *^4He vs. ^4Li and production of light nuclei in relativistic heavy-ion collisions*, Mod. Phys. Lett. **33**, 1850142 (2018); S. Mrowczynski, *Production of light nuclei in the thermal and coalescence models*, Acta Phys. Polon. B **48**, 707 (2017).
- [60] P. M. Lo and F. Giacosa, *Thermal contribution of unstable states*, arXiv:1902.03203 [hep-ph].
- [61] P. M. Lo, *S-matrix formulation of thermodynamics with N -body scatterings*, Eur. Phys. J. C **77**, 533 (2017).
- [62] X.H. He *et al.* (Belle Collaboration), *Observation of $e^+e^- \rightarrow \pi^+\pi^-\pi^0\chi_{bJ}$ and Search for $X_b \rightarrow \omega\Upsilon(1S)$ at $\sqrt{s} = 10.867 \text{ GeV}$* , Phys. Rev. Lett. **113**, 142001 (2014).
- [63] G. Aad *et al.* (ATLAS Collaboration), *Search for the X_b and other hidden-beauty states in the $\pi^+\pi^-\Upsilon(1S)$ channel at ATLAS*, Phys. Lett. B **740**, 199 (2015).
- [64] S. Chatrchyan *et al.* (CMS Collaboration), *Search for a new bottomonium state decaying to $\Upsilon(1S)\pi^+\pi^-$ in pp collisions at $\sqrt{s} = 8 \text{ TeV}$* , Phys. Lett. B **727**, 57 (2013).
- [65] R. Aaij *et al.* (LHCb Collaboration), *Observation of $\eta_c(2S) \rightarrow p\bar{p}$ and search for $X(3872) \rightarrow p\bar{p}$ decays*, Phys. Lett. B **769**, 305 (2017).